4-5-2023

Stabilizing Control Schemes for Grid-Connected Hybrid PV-Energy Storage Systems

Indra Narayana Bhogaraju
Louisiana State University and Agricultural and Mechanical College

STABILIZING CONTROL SCHEMES FOR GRID-CONNECTED HYBRID PV–ENERGY STORAGE SYSTEMS

A Dissertation

Submitted to the Graduate Faculty of the
Louisiana State University and
Agricultural and Mechanical College
in partial fulfillment of the
requirements for the degree of
Doctor in Philosophy

in

The Department of Electrical and Computer Engineering

by
Indra Narayana Sandilya Bhogaraju
B.Tech., GITAM University, 2015
M.S., University of Houston, 2017
May 2023

Acknowledgements

First and foremost, I would like to express my sincere gratitude to my esteemed advisor Dr. Mehdi Farasat for his invaluable supervision, continuous support, and patience at every stage of my research journey. He has been a mentor and a constant source of inspiration, and I am fortunate to have had the opportunity to work under his guidance. Next, I give special thanks to my co-advisor Dr. Michael Malisoff for his insightful comments, suggestions, and tutelage during my graduate studies.

Next, I would like to thank my committee members, Dr. Shahab Mehraeen, Dr. Amin Kargarian, Dr. Guoxiang Gu, and Dr. Luis A. Escobar, for their valuable suggestions and feedback. I also want to express my gratitude to the faculty and staff at the Division of Electrical Engineering for their support during my graduate studies. I sincerely thank all my lab mates, friends, and especially my roommates for the cherished time spent together and constant support throughout my journey.

There are no words to convey my sincere gratitude and respect for my parents for their unwavering support and endless patience. It was their unconditional love that raised me again when I had setbacks. There is no way to express how much it meant to have a caring and supportive brother like Koundinya Bhogaraju, whose love and affection have been with me throughout my life. I would also like to thank my sister-in-law for her care and support. Without my family's tremendous understanding and encouragement, it would be impossible for me to complete my Ph.D.

Table of Contents

Abstract

A nonlinear stabilizing control scheme based on Lyapunov theory is proposed for a grid-connected hybrid photovoltaic (PV)/ battery/supercapacitor (SC) system. The system dynamics is developed in the stationary reference frame, and the state-space model of the system is derived and used to formulate the Lyapunov function (LF) candidate. The global asymptotic stability of the LF-based controller is discussed in detail. The real-time implementation feasibility of the proposed control scheme is validated through hardware-in-the-loop (HIL) studies of a grid-connected hybrid system under solar energy generation and grid load variations. To address the issue of digital computational time that leads to delays in the grid-connected systems control, a novel delay-compensating stabilizing feedback is provided. The proposed control is based on delay-compensating chain predictors for bilinear systems, and it features real-time implementation feasibility and global asymptotic stability to desired reference trajectories. Real-time simulation results of a grid-connected PV/battery/SC verify the efficacy of our method in controlling its dynamics in the presence of digital implementation delays while ensuring the delivery of desired power to the grid.

Chapter 1. Introduction

The adversary effects of fossil fuel-based conventional power systems on the environment have caused a global shift in research toward grid integration of renewable energy sources (RESs). These RESs have become the beacon of hope for a sustainable future because of their resilience, sustainability, energy security, economic feasibility, and environmental benefits. Owing to technological advancements in the field of power electronics and semiconductor devices, grid integration of RESs has become increasingly feasible in recent years. RESs, such as solar, wind, and ocean power, contribute to a significant amount of energy generation and act as an alternative to fossil fuels. Power electronic converters act as the bridge for interfacing RESs with the grid [1]. Due to the stochastic and intermittent nature of RESs, there is an inevitable need to utilize energy storage systems (ESS). These ESSs are needed to compensate for the intermittency and variability of RESs that may lead to grid instability and affect reliability.

The main purpose of ESSs is to aid RESs in enhancing reliability. Battery energy storage, pumped storage, flywheel-based energy storage, compressed air energy storage, thermal energy storage, and supercapacitor-based energy storage are some of the most commonly used ESSs in the present-day market. Table 1 summarizes different types of ESSs, their advantages, disadvantages, and applications.

The battery-supercapacitor (SC) HESS is increasingly becoming popular as it features high energy and power density thanks to the battery and SC, respectively. In addition, an efficient energy management strategy can provide a smooth power profile for the battery, leading to its extended lifetime.

Table 1.1. Summary of different energy storage systems

Type of ESS	Applications	Advantages	Disadvantages
Battery	Portable devices like mobile, laptop charges, regulate grid fluctuations, electric vehicles	High energy density, high efficiency, proven technology, easy accessibility, wide range of energy capacities	Low power density, high maintenance, slow response times, high costs, limited resources, heating issues
Supercapacitors	Regulate peak load grid fluctuations, rapid energy applications, supplements to batteries in electric vehicles	High power density, high efficiency, low maintenance, easy to integrate with other storage systems	Low energy density, low energy capacity, high discharge rates
Pump storage	Large scale energy storage, during peak demands	High efficiency, energy trading, reliability, high energy capacity	High maintenance, geographical requirements, high costs
Flywheel	Electric vehicles, regulate power supply in semiconductor manufacturing	Low cost, high power density, easy and fast access, reliability	High maintenance, problems with self-discharge, limited energy storage
Compressed-air storage	Peak shaving, grid stability	Low operating costs, long life span	High losses, low efficiency, complex to integrate with RESs
Thermal storage	Solar thermal power plants, thermo chemical storage systems	Peak demands, robustness	Hazardous, high maintenance, high costs, high losses

It can be seen from Table 1 that none of the ESSs possesses all the desirable qualities of an ideal ESS. Therefore, a hybrid energy storage system (HESS) comprised of a battery that has high energy density and a supercapacitor (SC) that has high power density can be a viable solution to energy storage [2].

Voltage source inverters (VSI) are the enabling technology for integrating and interfacing RESs with the grid. Control of VSI has been the topic of interest for researchers in the field of

power electronics in the past few decades and has been extensively studied in the literature. Grid-connected photovoltaic VSI with HESS comprising battery and supercapacitor can be a promising solution to meet energy demands, extend battery life, and maintain grid stability. In these systems, the control objective is to regulate current, voltage, and power.

Different topologies with new strategies have been proposed to control VSI and HESS in the literature. The most popular controllers used are conventional proportional integral-based controllers, sliding mode controllers [3], model predictive controllers [4], and observer-based controllers [5]. While most of these controllers focus on the system performance, very few present a detailed stability analysis. Motivated by this lack of studies, chapter 2 presents a Lyapunov function-based control scheme for a grid-connected hybrid PV/batter/supercapacitor system.

Control schemes of grid-connected VSIs/HESS are implemented on digital signal processors (DSPs). The analog current and voltage measurements are sent into DSP. After being processed following the control algorithm, control inputs are generated in the form of switching pulses through a pulse width modulator. The time for analog-to-digital conversion and control signal generation, which is known as digital implementation time, will lead to time delays that can cause stability issues in the system [6]. The complexity of the control algorithm directly affects the control signal generation time, i.e., computational time. Digital implementation delays in power electronics converter control due to computational complexity can have a detrimental effect on stability and system performance. In the literature, various works have been proposed that can compensate for arbitrarily long input delays. Still, these control techniques can pose a problem because of their complexity which can, in turn, increase the computational time delay. This motivated the development of the concept of sequential predictors for delay compensation.

Chapter 3 presents a novel control technique based on sequential predictors for delay compensation in bilinear systems with uncertainties. Chapter 4 presents the application of the theory developed in Chapter 3 for constructing a delay-compensating stabilizing feedback controller for a grid-connected PV/hybrid energy storage system. Conclusions and future study plans are presented in Chapter 5.

Chapter 2. Lyapunov Function-Based Stabilizing Control Scheme for a Grid-Connected Hybrid PV/Battery/Supercapacitor System

2.1. Introduction

Although renewable energy sources (RESs), such as photovoltaic (PV) and wind energy conversion systems, offer significant environmental benefits, they are associated with the disadvantage of non-uniform and fluctuating energy and voltage outputs due to uncertainties and variations in the environmental conditions [7]. With higher penetration of RESs, energy storage systems (ESSs) are needed to ensure power backup and enhance power flexibility in the power grid. A hybrid energy storage system (HESS), a combination of two or more ESSs with complementary characteristics, is an environmentally friendly alternative suited to address drastic load fluctuations, thus leading to efficient management of power. The battery-supercapacitor (SC) HESS is increasingly becoming popular as it features high energy and power density thanks to the battery and SC, respectively. In addition, an efficient energy management strategy can provide a smooth power profile for the battery, leading to its extended lifetime.

To improve the grid current quality at mid- and high-power applications, an inductor-capacitor-inductor (LCL) filter must be placed between the grid and the inverter. Therefore, this work considers such a filter at the output of the three-phase grid-connected PV inverter. In grid-connected converters, the common control objective is to regulate voltage, current, or power. Several works in the literature propose different approaches to achieve this goal. The sliding-mode control (SMC) has shown features such as simple implementation and robustness against external disturbances and system parameter variations. In [8], a linearized model of the three-phase inverter with an LCL filter is used to design a pulse width modulation (PWM) based SMC. Thanks to linearization, simplified switching is achieved, and determining a stability region based on

classical control theory is made possible. However, the frequent change in sliding gain results in weak dynamic response during load variations. In addition, PWM-based-SMC suffers from steady-state errors in voltage output. In [9], a modified SMC that eliminates the need for filter capacitor voltage and grid current sensing is proposed. The proposed method also eliminates an additional term in the sliding surface function, commonly used to reduce the grid current error. However, a complete stability analysis that ensures global asymptotic stability needs to be provided. Another promising control strategy for grid-connected converters that has been extensively studied in the literature is model predictive control (MPC) [4].

In [10], the issues that arise with the use of voltage sensors in conventional control techniques like direct-power control, grid voltage-oriented control, and direct current control is discussed, and an MPC strategy for grid-connected inverters without using ac voltage sensors is proposed. To achieve sensor less control, L. Guo et al. designed a sliding-mode observer to estimate the grid voltages, thereby mitigating costs associated with voltage sensors. Despite these advantages, one major drawback of the MPC is the computational burden, which becomes a significant problem in duty ratio modulated, multiple-vector MPC, and multilevel converters. To overcome this issue, E. T. Andrew et al. proposed a duty ratio modulated model predictive current controller that reduces the computational burden by half using an extended complex Kalman filter (ECKF) [11]. In addition to computational complexity, other disadvantages of MPC-based strategies are sensitivity to system parameter variations and degraded dynamic performance in case of load variations. Disturbance observer-based controllers are commonly used to improve dynamic performance [5]. In [12], a disturbance observer combined with a state feedback controller is proposed to compensate for the current disturbances caused by the variations in load resistance and inductance. However, the controller is designed only to compensate for sinusoidal disturbances with a known

frequency. A disturbance observer based robust MPC is proposed in [13] to minimize voltage sensors and improve dynamic performance. In summary, control strategies based on disturbance observers require accurate modeling, and their efficacy is highly dependent on the accurate knowledge of the parameters. Also, constructing a disturbance observer adds to the control complexity, leading to additional computational time delay. Very few works can be found in the literature that can ensure system stability, ease of implementation, and enhanced performance while offering robustness to parameter variations.

The Lyapunov function (LF)-based control methods have been implemented in various works in the literature due to features such as asymptotic stability of the equilibrium, robustness against load and parameter variations, and ease of implementation. Due to these advantages, LF-based approaches are used to regulate single-phase [14], [15] and three-phase ac/dc rectifiers [16], multilevel inverters [17], neutral point clamped converters [18], dc/dc converters [19], grid-connected inverters and shunt active power filters [20], [21]. Ref [22] is one of the first works where an LF-based control strategy is implemented for power electronics systems, i.e., a buck/boost dc/dc converter. An LF-based control is implemented for single-phase grid-connected PV inverters in [15] that not only ensures the global stability of the closed loop system but also provides robustness against solar irradiance uncertainties. However, the robustness of the proposed LF-based strategies in [15], [17]-[19] is only against small ranges, and large disturbances can still affect the system's stability. To address this issue, [16] proposed a control technique based on Lyapunov's stability theory and applied it to three-phase rectifiers. The proposed method provides global asymptotic stability (GAS) and robustness against large-scale disturbances.

The majority of the LF-based approaches for three-phase inverters are single-loop control systems, where current is controlled by placing the system poles near the imaginary axis. This

leads to system instability with a slight margin for robustness against disturbances or parameter variations. To overcome this drawback, [22] presented an enhanced LF-based control, where a second loop with filter capacitor voltage feedback is added to improve the damping performance. The addition of the second loop improves reference tracking of the grid currents. However, the non-strictness of the Lyapunov function, which is the major factor in guaranteeing GAS, is not addressed. In [23], an LF-based control for a grid-connected three-phase inverter with a battery energy storage system is presented. However, the battery reference current is obtained as the output of a proportional-integral (PI) controller, which is a time-varying quantity. At the same time, the presented analysis considers references as constant values. An LF-based method is proposed in [24] for controlling the distrusted energy resources in a hybrid ac/dc microgrid. However, like [22], the non-strictness of the Lyapunov function is not addressed. Ref [25], where an LF-based controller is proposed for wireless charging of electric vehicles, is one of the very few works that addressed the issue of achieving GAS with a non-strict Lyapunov function.

To address the abovementioned drawbacks, in this work, we propose a stabilizing feedback controller for a grid-connected hybrid PV/battery/SC system. As shown in Figure. 2.1, the PV system is interfaced with the grid using a three-phase inverter with an LCL filter at its output. The battery and SC are interfaced with the dc-link capacitor of the inverter using individual bidirectional buck/boost dc/dc converters. The major contributions of this work are twofold:

- Global asymptotic stability of the feedback controller for a grid-connected hybrid PV/battery/SC system is guaranteed. The controller is designed based on Lyapunov theory, and the non-strictness of the Lyapunov function is discussed and addressed in detail using LaSalle's invariance argument.

- The real-time implementation feasibility of the proposed controller is verified through hardware-in-the-loop (HIL) studies, where the PV, battery, SC, dc/dc converters and their control, and the inverter are modeled on an OP4510 real-time simulator from Opal-RT Technologies, and the inverter's control is implemented on a TMS320F28335 digital signal processor (DSP).

The paper is organized as follows. The hybrid PV/battery/SC system model is presented in Section II. The feedback controller with stability analysis based on Lyapunov theory is discussed in Section III. HIL results and discussions are provided in Section IV, and conclusions are drawn in Section V.

2.2. Hybrid PV/battery/SC system model

2.2.1. System Description

Figure. 2.1 shows the schematic of a typical Three-phase grid-connected PV inverter with HESS. The PV source is modeled as a controlled current source and is connected to the three-phase inverter via a dc-link capacitor. An LCL filter connects the three-phase inverter to the grid. The control signals are the PWM signals for the three-phase inverter and both the battery and SC bi-directional dc/dc converters.

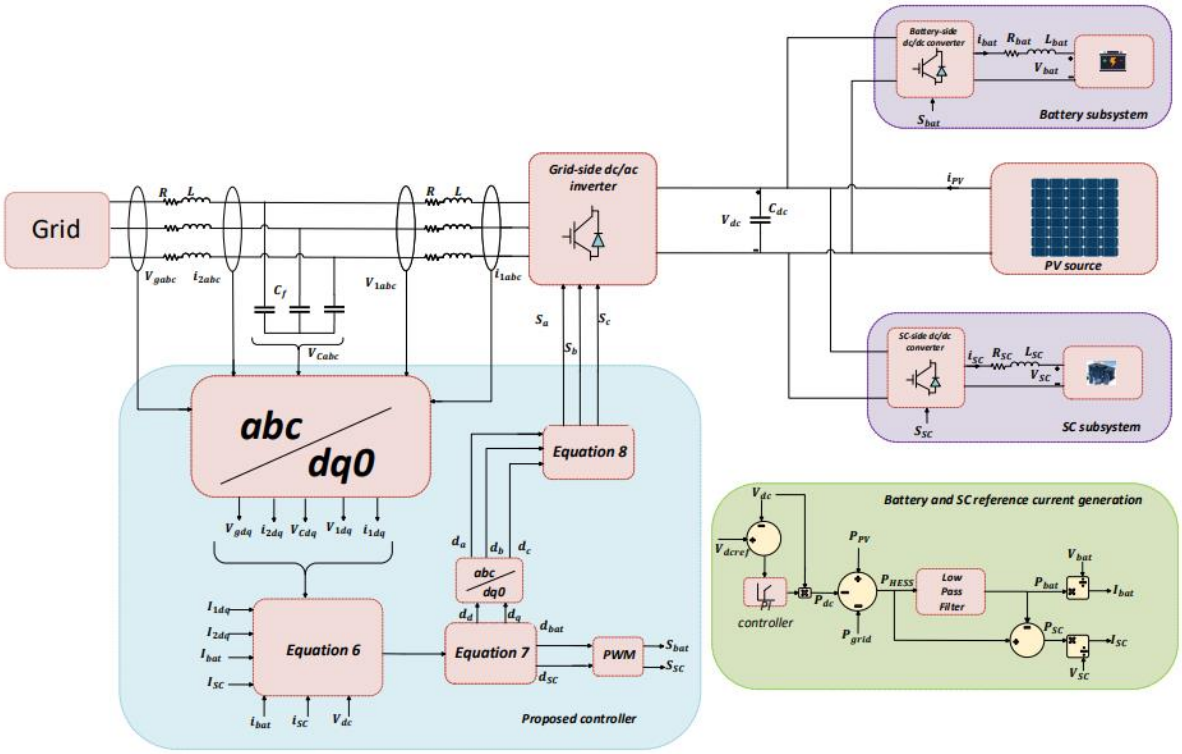

Figure. 2.1. PV/HESS system circuit diagram and control scheme.

2.2.2. System Dynamics

The dynamics of the system in Figure. 2.1 are expressed as,

$$L\frac{di_{1d}}{dt} = \frac{1}{2}d_d V_{dc} - V_{Cd} + \omega L i_{1q} - R i_{1d}$$

$$L\frac{di_{1q}}{dt} = \frac{1}{2}d_q V_{dc} - V_{Cq} - \omega L i_{1d} - R i_{1q}$$

$$L\frac{di_{2d}}{dt} = V_{Cd} - V_{gd} + \omega L i_{2q} - R i_{2d}$$

$$L\frac{di_{2q}}{dt} = V_{Cq} - V_{gq} - \omega L i_{2d} - R i_{2q}$$

$$C_{dc}\frac{dV_{dc}}{dt} = i_{pv} - \frac{3}{4}d_d i_{1d} - \frac{3}{4}d_q i_{1q} - d_{bat} i_{bat} - d_{SC} i_{SC}$$

$$L_{bat}\frac{di_{bat}}{dt} = d_{bat}V_{dc} - V_{bat} - R_{bat}i_{bat}$$

$$L_{SC}\frac{di_{SC}}{dt} = d_{SC}V_{dc} - V_{SC} - R_{SC}i_{SC}$$

$$C_f\frac{dV_{Cd}}{dt} = i_{1d} - i_{2d} + \omega C_f V_{Cq}$$

$$C_f\frac{dV_{Cq}}{dt} = i_{1q} - i_{2q} - \omega C_f V_{Cd} \quad (1)$$

whose derivation and notation are as follows.

The dynamics (1) are obtained using Kirchhoff's voltage and current laws and are expressed in the synchronously rotating dq0 reference frame, which are dc quantities, using Park's transformation [26, Appendix 3]. The reference q-component of the grid voltage and current, as well as the grid reactive power, can be set to 0. The battery and SC can be modeled as voltage sources with series resistances for mathematical analysis. The inverter currents in the dq0 frame, grid currents in dq0 frame, filter capacitor voltages in dq0 frame, dc-link voltage, and battery and SC currents are selected as state variables for the control system design. Here, i_{pv} denotes the current value of the PV source, and d_a, d_b, and d_c are inverter switching functions in the abc frame and are transformed into d_d and d_q using Park's transformation. V_{ga}, V_{gb}, and V_{gc} are the grid three-phase voltages and V_{gd}, and V_{gq} are the dq components of the grid voltage, i_{2a}, i_{2b}, and i_{2c} are the grid three-phase currents and i_{2d} and i_{2q} are the dq components of the grid current, i_{1a}, i_{1b}, and i_{1c} are the inverter three-phase currents and i_{1d} and i_{1q} are the dq components of the inverter current, V_{Ca}, V_{Cb}, and V_{Cc} are the capacitor filter three-phase voltages and V_{Cd} and V_{Cq} are the dq components of the capacitor filter voltage. d_{bat} and d_{SC} are duty ratios of the dc/dc converters of the battery and SC, respectively. Real valued V_{bat}, V_{SC}, i_{bat}, i_{SC}, and V_{dc} are the

battery voltage, SC voltage, battery current, SC current, and dc-link voltage, respectively, and are expressed using the following relations:

$$V_{bat} = V_{ob} - i_{bat}R_b \quad \text{and} \quad V_{SC} = V_{os} - i_{SC}R_s \tag{2}$$

Here, $V_{ob}$and R_b are the internal voltage and resistance of the battery, respectively, and V_{os} and $R_s$are the internal voltage and resistance of the SC, respectively. The constants $L$and R and are the line resistance and inductance and are real valued. The known real valued constants $L_{bat}$and R_{bat} are the battery inductance and resistance, respectively, the known real valued constants $L_{SC}$and R_{SC} are the SC inductance and resistance, respectively, the known real valued constants C_{dc} and C_f are the dc-link and filter capacitance, respectively, and the known constant ω is the grid angular frequency. The constants $L_{bat}, R_{bat}, R_{SC}, L_{SC}, C_{dc}, i_{PV}, V_{ob}, V_{os}, C_f, L, R$, and ω are positive, and the constants V_{gd}, V_{gq}, R_s, and $R_b$are non-negative.

We next represent the steady state model at a time-varying reference solution to formulate our stabilization problem. These reference state currents and voltages are reference values for the state variable candidates in (1) and so must satisfy

$$L\frac{dI_{1d}}{dt} = \frac{1}{2}D_d V_{dcref} - V_{Cdref} + \omega L I_{1q} - RI_{1d}$$

$$L\frac{dI_{1q}}{dt} = \frac{1}{2}D_q V_{dcref} - V_{Cqref} - \omega L I_{1d} - RI_{1q}$$

$$L\frac{dI_{2d}}{dt} = V_{Cdref} - V_{gd} + \omega L I_{2q} - RI_{2d}$$

$$L\frac{dI_{2q}}{dt} = V_{Cqref} - V_{gq} - \omega L I_{2d} - RI_{2q}$$

$$C_{dc}\frac{dV_{dcref}}{dt} = i_{pv} - \frac{3}{4}D_d I_{1d} - \frac{3}{4}D_q I_{1q} - D_{bat}I_{bat} - D_{SC}I_{SC}$$

$$L_{bat}\frac{dI_{bat}}{dt} = D_{bat}V_{dcref} - V_{bat\_s} - R_{bat}I_{bat}$$

$$L_{SC}\frac{dI_{SC}}{dt} = D_{SC}V_{dcref} - V_{SC\_s} - R_{SC}I_{SC}$$

$$C_f\frac{dV_{Cdref}}{dt} = I_{1d} - I_{2d} + \omega C_f V_{Cqref}$$

$$C_f\frac{dV_{Cqref}}{dt} = I_{1q} - I_{2q} - \omega C_f V_{Cdref} \quad (3)$$

where capitalization of letters or subscripts ref or_s indicate the corresponding reference values that correspond to the variables in (1), so for instance,

$$V_{bat\_s} = V_{ob} - I_{bat}R_b \text{ and } V_{SC\_s} = V_{os} - I_{SC}R_s \quad (4)$$

The state variables are chosen as the errors between the actual measured quantities and their reference values

$$x_1 = i_{1d} - I_{1d}$$

$$x_2 = i_{1q} - I_{1q}$$

$$x_3 = i_{2d} - I_{2d}$$

$$x_4 = i_{2q} - I_{2q}$$

$$x_5 = V_{dc} - V_{dcref}$$

$$x_6 = i_{bat} - I_{bat}$$

$$x_7 = i_{SC} - I_{SC}$$

$$x_8 = V_{Cd} - V_{Cdref}$$

$$x_9 = V_{Cq} - V_{Cqref} \tag{5}$$

By (1) – (5), we obtain error dynamics as

$$L\dot{x}_1 = \frac{1}{2}\left(\Delta d_d\left(x_5 + V_{dcref}\right) + D_d x_5\right) - x_8 + \omega L x_2 - R x_1$$

$$L\dot{x}_2 = \frac{1}{2}\left(\Delta d_q\left(x_5 + V_{dcref}\right) + D_q x_5\right) - x_9 - \omega L x_1 - R x_2$$

$$L\dot{x}_3 = x_8 + \omega L x_4 - R x_3$$

$$L\dot{x}_4 = x_8 - \omega L x_3 - R x_4$$

$$C_{dc}\dot{x}_5 = -\frac{3}{4}(\Delta d_d(x_1 + I_{1d}) + D_d x_1) - \frac{3}{4}\left(\Delta d_q\left(x_2 + I_{1q}\right) + D_q x_2\right) - (\Delta d_{bat}(x_6 + I_{bat}) + D_{bat} x_6) - (\Delta d_{SC}(x_7 + I_{SC}) + D_{SC} x_7)$$

$$L_{bat}\dot{x}_6 = \left(\Delta d_{bat}\left(x_5 + V_{dcref}\right) + D_{bat} x_5\right) - \Delta V_{bat} - R_{bat} x_6$$

$$L_{bat}\dot{x}_7 = \left(\Delta d_{SC}\left(x_5 + V_{dcref}\right) + D_{SC} x_5\right) - \Delta V_{SC} - R_{SC} x_7$$

$$C_f\dot{x}_8 = x_1 - x_3 + \omega C_f x_9$$

$$C_f\dot{x}_9 = x_2 - x_4 - \omega C_f x_8 \tag{6}$$

where

$$\Delta V_{bat} = V_{bat} - V_{bat\_s} \quad \text{and} \quad \Delta V_{SC} = V_{SC} - V_{SC\_s}$$

In (6), the control inputs are the switching functions for the three-phase inverter in the dq0 frame, and the switching states for the battery and SC's dc/dc converters. The terms Δd_d, Δd_q, Δd_{bat}, and Δd_{SC} are the differences between control and reference values, i.e.,

$$u_1 = \Delta d_d = d_d - D_d$$

$$u_2 = \Delta d_q = d_q - D_q$$

$$u_{bat} = \Delta d_{bat} = d_{bat} - D_{bat}$$

$$u_{SC} = \Delta d_{SC} = d_{SC} - D_{SC} \quad (7)$$

where,

$d_k = S_k - \frac{S_a+S_b+S_c}{3}$ for $k = a, b,$ and $c,$

$$d_{bat} \xrightarrow{PWM} S_{bat} \text{ and } d_{SC} \xrightarrow{PWM} S_{SC} \quad (8)$$

The switching states on the right sides of (8) are the gating signals generated by PWM. The control inputs u_i are chosen such that (6) satisfies a global asymptotic stability property in the sense of Lyapunov which will be explained in the coming sections.

2.2.3. HESS

The surplus or the deficit of the PV power in comparison to constant grid power is absorbed or provided by the battery/SC HESS. The sudden changes in the battery power profile adversely affect its lifetime. To reduce stress on the battery and lengthen its lifespan, the SC is assigned the role of handling sudden variations, while the battery's role is to provide smooth energy flow over long time periods. To achieve this, P_{HESS} is passed through a low-pass filter (or LPF). The low-frequency output component of the LPF is assigned as the reference power that must be supplied/absorbed by the battery, P_{bat}, and the high-frequency component is assigned as the reference power that the SC must supply/absorb, P_{SC}. Once the battery and SC reference powers are determined, the reference battery and SC currents, which are the reference states in (3), are then readily determined by dividing the reference powers by the corresponding voltages. The LPF-based algorithm shown in Figure 2.1., as described above, is applied to obtain the HESS power

and, thereby, battery and SC current references. An LCL filter is chosen to effectively smooth the inverter current output and supply filtered harmonic-free current to the grid. It also offers high attenuation, good harmonic elimination, improved performance, and cost-effectiveness with low inductors and capacitors values.

The HESS includes a battery and an SC, each with its individual bidirectional dc/dc buck-boost converter. The flow of HESS power, P_{HESS}, is controlled through the PWM signals that are sent to the dc/dc converters interfacing the battery and SC and are obtained by $P_{HESS} = P_{PV} - P_{dc} - P_g$, where P_{PV}, P_{dc}, and P_g are the PV, dc-link, and grid power, respectively. This relationship is in accordance with the power balance principle at the dc link, i.e., the PV power entering the dc link is the sum of the powers delivered to the grid, the HESS, and the dc-link capacitor. To achieve proper operation of the dc/ac inverter, it is crucial to maintain the dc-link voltage, V_{dc}, constant at a reference value. As seen in Figure. 2.1, this is achieved by employing a PI controller and regulating the dc-link power, P_{dc}. The PWM signals are switching states averaged over one time period and defined in (8).

It can be seen from (1) that the three-phase grid-connected inverter consists of 9 states, x_1-x_9. Thus, for reference waveform tracking for all the states, a nonlinear control law is derived based on the Lyapunov theory.

2.3. Lyapunov Function-Based Feedback Controller

This section explains the employment of the Lyapunov function-based control strategy to perform multifunctioning objectives, i.e., ensure global stability of the system equilibrium, maintain constant DC link voltage, injection of sinusoidal inverter current to the utility grid, and improved power quality to the grid. It can reduce the higher switched frequency of inserting LCL

(Passive) filter between the inverter and the utility grid. The active currents are controlled to inject stable power to utility grid. Consider a system that is defined by

$$\dot{x} = f(x)\,, \qquad x \in \mathbb{R}^n \tag{9}$$

The Global Asymptotic Stability (GAS) of the equilibrium of the nonlinear system is guaranteed if the chosen Lyapunov function candidate, $V(x)$ satisfies the following conditions,

$$V(0) = 0$$

$$V(x) > 0 \;\; for\; all\; x \neq 0$$

$$V(x) \to \infty \;\; as \;\; ||x|| \to \infty$$

$$\dot{V}(x) < 0 \;\; for\; all\; x \neq 0 \tag{10}$$

Now, consider the following energy-like Lyapunov function for the system in (1)

$$V(x) = \frac{1}{2}Lx_1{}^2 + \frac{1}{2}Lx_2{}^2 + \frac{1}{2}Lx_3{}^2 + \frac{1}{2}Lx_4{}^2 + \frac{1}{2}C_{dc}x_5{}^2 + \frac{1}{2}L_{bat}x_6{}^2 + \frac{1}{2}L_{SC}x_7{}^2 + \frac{1}{2}C_f x_8{}^2 + \frac{1}{2}C_f x_9{}^2 \tag{11}$$

The preceding conditions, in conjunction with the LaSalle invariance argument [28], will ensure GAS of (6) to the origin. It can be seen that $V(x)$ satisfies the first three conditions in (10). The control law is derived by satisfying the last negative definiteness condition. The time derivative of (11) along (6) is obtained as follows:

$$\dot{V}(x) = Lx_1\dot{x}_1 + Lx_2\dot{x}_2 + Lx_3\dot{x}_3 + Lx_4\dot{x}_4 + C_{dc}x_5\dot{x}_5 + L_{bat}x_6\dot{x}_6 + L_{SC}x_7\dot{x}_7 + C_f x_8\dot{x}_8 + C_f x_9\dot{x}_9 \tag{12}$$

After some simplifications, Lyapunov function derivative will become,

$$\dot{V}(x) = \left(-\mathrm{R}{x_1}^2 - \mathrm{R}{x_2}^2 - \mathrm{R}{x_3}^2 - \mathrm{R}{x_4}^2 - R_{bat}{x_6}^2 - R_{SC}{x_7}^2 + \Delta V_{bat}x_6 + \Delta V_{SC}x_7 - \right.$$

$$\Delta d_d\left(x_1 V_{dcref} - x_5 I_{1d}\right) - \Delta d_q\left(x_2 V_{dcref} - x_5 I_{1q}\right) - \Delta d_{bat}(x_6 V_{dcref} - x_5 I_{bat}) -$$

$$\left.\Delta d_{SC}(x_7 V_{dcref} - x_5 I_{SC})\right) \quad (13)$$

For satisfying the negative definiteness condition, i.e., $\dot{V}(x) < 0$, the control inputs are chosen as,

$$\Delta d_d = K_{\mathrm{d}}(x_1 V_{dcref} - x_5 I_{1d})$$

$$\Delta d_q = K_{\mathrm{q}}(x_2 V_{dcref} - x_5 I_{1q})$$

$$\Delta d_{bat} = K_{\mathrm{bat}}(x_6 V_{dcref} - x_5 I_{bat})$$

$$\Delta d_{SC} = K_{\mathrm{SC}}(x_7 V_{dcref} - x_5 I_{SC}) \quad (14)$$

where $K_{\mathrm{d}}, K_{\mathrm{q}}, K_{\mathrm{bat}}, K_{\mathrm{SC}} > 0$

It is noteworthy to mention that (16) can only achieve $\dot{V}(x) \leq 0$. This is a special case where we have a non-strict Lyapunov function (which allows nonzero values of the state x where, $\dot{V}(x) = 0$) and the analysis involving the control inputs in (16) is insufficient to achieve GAS of the equilibrium point of (6). To prove the dynamical system's equilibrium is GAS, we employ LaSalle's invariance argument. $\dot{V}(x) = 0$, implies that, $x_1 = 0, x_2 = 0, x_3 = 0, x_4 = 0, x_6 = 0, x_7 = 0$. Substituting these values in (6) will render $x_5 = 0, x_8 = 0$, and $x_9 = 0$. As it is shown that $x = 0$, the GAS property follows from LaSalle's invariance principle.

2.4. Results and Discussion

Real-time performance of the three-phase grid connected PV inverter working along with the HESS is investigated on a HIL setup to verify the effectiveness of the proposed LF-based controller in tracking the reference power to be injected to the grid. The HIL setup consists of an OP4510

real-time simulator from Opal-RT Technologies, Inc., operating with a Kintex7 field-programmable gate array (or FPGA) and a TI TMS320F28335 DSP. The entire system, including the grid, LCL filter, PV source, and the HESS, and the control for the HESS are modeled on the real-time simulator, while the inverter control is implemented on the TI DSP. Table 1 summarizes the system and control parameters.

The grid reference power is initially set at 25 kW. Then, the reference power is increased with a step change of 12.5 kW at t=4s, following a step decrease of 18.75 kW at t=7s. Figure. 2.2 depicts the PV, battery, SC, and grid power profiles. The PV power profile is obtained by using real solar data from the US National Renewable Energy Laboratory (NREL). As can be seen, the grid power follows the reference accurately and with fast dynamics at step change instants. It is noteworthy to mention that thanks to the LPF, the battery power is smooth and does not contain high surges and transients similar to those that are present in the SC's power profile.

The dc-link voltage and the three-phase grid currents are depicted in Figure. 2.3. The dc-link voltage is maintained at the reference value of 650V, confirming that the power balance is maintained. The same changes can be observed in the grid three-phase currents, showing the increase and decrease in the power delivered to the grid. The nine state variables are plotted in Figure. 2.4. The system states converge to zero in a reasonably short period of time, confirming fast convergence of the error dynamics and that all the current and voltage measurements are tracking their reference values effectively.

The entire system, including the grid, LCL filter, PV source, and the HESS, and the control for the HESS are modeled on the real-time simulator, while the inverter control is implemented on the TI DSP. Table 1 summarizes the system and control parameters.

Table 2. System parameters in Real-time simulations

Parameter	Value
R [Ω]	0.5
L [H]	0.012
R_{bat} [Ω]	0.06
L_{bat} [H]	0.005
R_{SC} [Ω]	0.08
L_{SC} [H]	0.001
V_{gd} [V]	300
V_{gq} [V]	0
V_{ob} [V]	300
V_{os} [V]	300
R_b [Ω]	0.0008
R_s [Ω]	0.0006
i_{pv} $[amp]$	42.30
ω $[rad/\sec]$	377
V_{dcref} [V]	650
C_{dc} $[F]$	0.0047
C_f $[F]$	0.000025
K_d	0.0315
K_q	0.4525
K_{bat}	2.85
K_{SC}	0.0015
$f_{sw}[Hz]$	10000

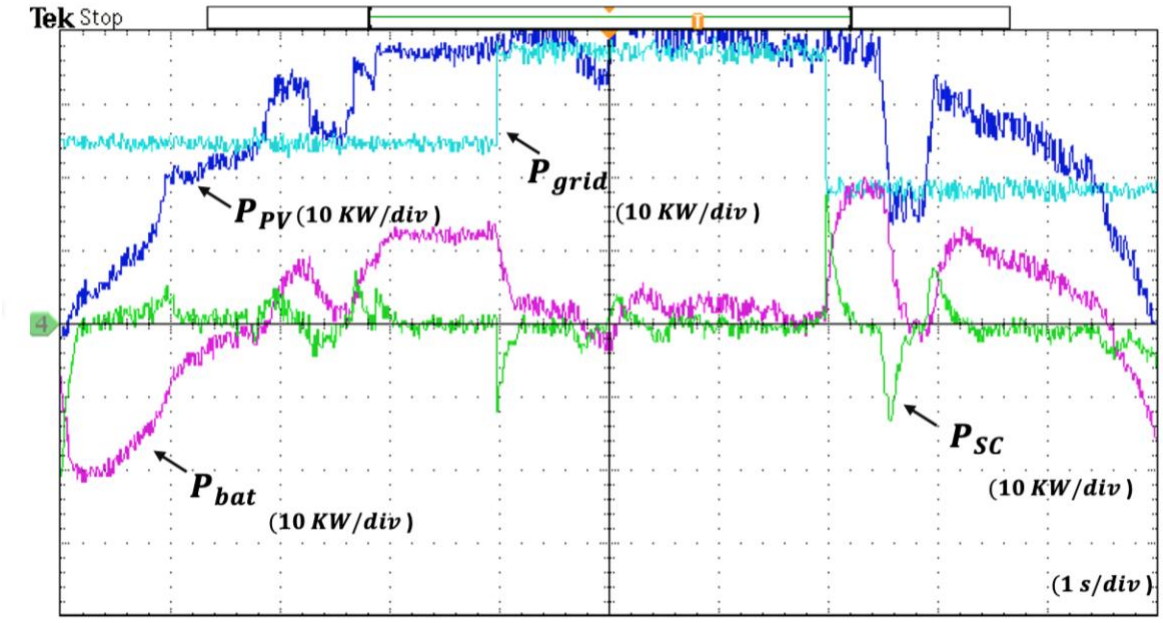

Figure. 2.2. Real time power profiles of PV, grid, battery, and SC

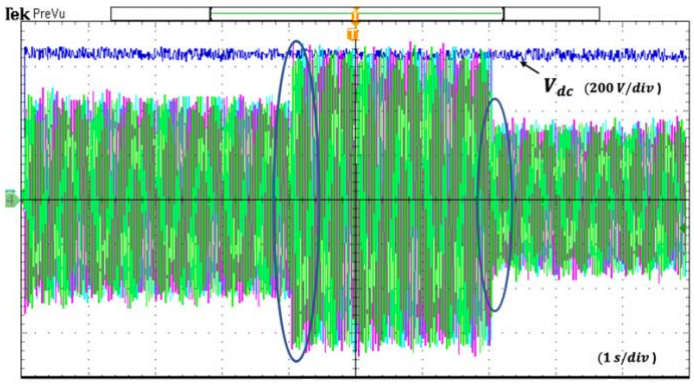

(a)

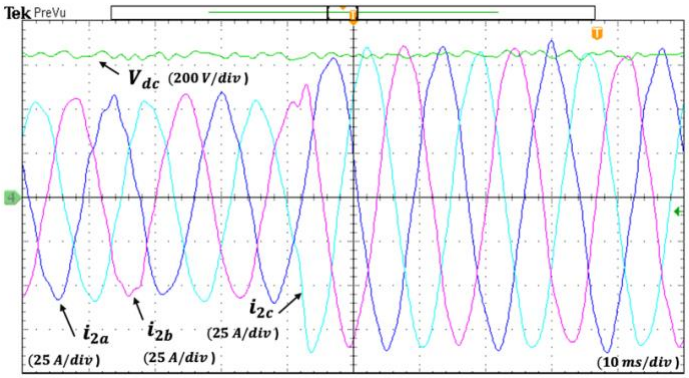

(b)

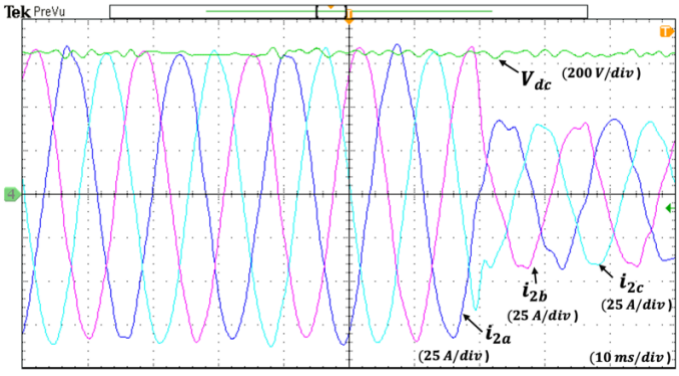

(c)

Figure. 2.3. Real time dc-link voltage and three-phase grid currents. (b) Zoomed in view of the first circled area in (a) showing step change at 4 seconds. (c) Zoomed in view of the second circled are showing step change at 7 seconds.

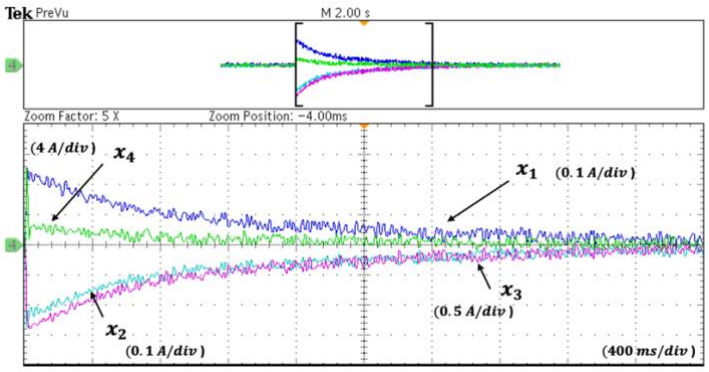

(a)

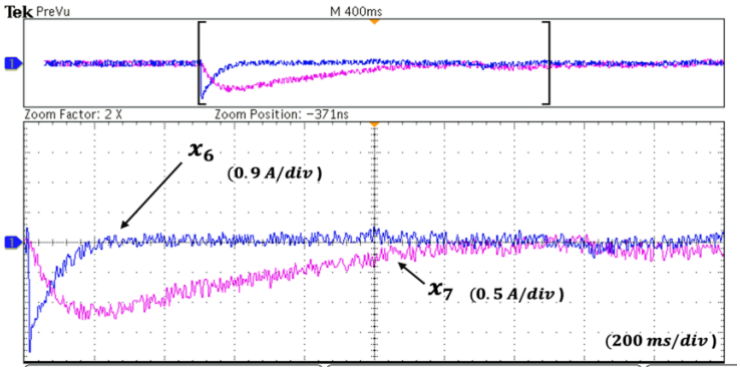

(b)

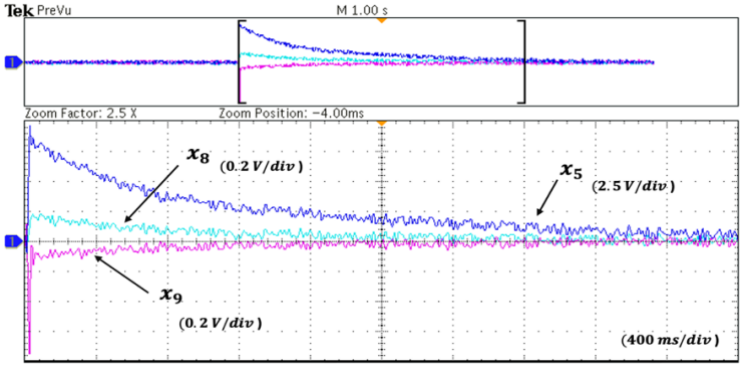

(c)

Figure. 2.4. Real time state responses. (a) states 1,2,3, and 4. (b) states 6 and 7. (c) states 5,8, and 9.

2.5. Conclusion

The state-space model of the grid-connected PV/battery/SC system with an LCL filter at the PV inverter's output is derived, showing that the hybrid system is bilinear. Therefore, a novel LF-

based control scheme is designed. Despite a non-strict Lyapunov function candidate, using LaSalle's invariance argument, it is shown that the GAS of the system equilibrium can be achieved. HIL studies are conducted to show the real-time implementation feasibility and dynamic response of the proposed feedback controller. The HIL results verify the effectiveness of the proposed controller in providing accurate power reference tracking, ensuring delivery of the desired power to the grid under solar source output energy and load variations.

Chapter 3. Sequential Predictors for Delay-Compensating Feedback Stabilization of Bilinear Systems with Uncertainties

3.1. Introduction

This chapter continues the development (which started, e.g., in [27–29] and [30]) of sequential predictor approaches for compensating for arbitrarily long input delays. Prior results covered dynamics whose right sides satisfy a linear growth condition. Here we cover feedback designs for dynamics for which this linear growth condition is not needed, and which therefore can be applied to important bilinear systems that were beyond the scope of previous sequential predictor methods; see [31–33] for the value of bilinear systems. Our method is motivated by the ubiquity of input delays in many applications, and the bottlenecks that arise when using standard controllers that were not designed to compensate for the input delays; see [34–43].

A natural method for coping with input delays is emulation, which calls for designing stabilizing feedback that can be applied when the input delays are zero, and where one then calculates a bound on the input delays under which the resulting closed loop system still enjoys desired global asymptotic stability properties; see, e.g., [46].

These other methods can compensate for arbitrarily long input delays but can be complicated to use in practice because their controls are only implicitly defined as solutions of integral equations; see, for instance [45,46], and [47]. This motivated [27] and [28] and other papers on sequential predictors for delay compensation, which normally express the control using values of an auxiliary variable that is viewed as an output of a collection of ordinary differential equations.

This chapter was previously published as I. Bhogaraju, M. Farasat, M. Malisoff, and M. Krstic, "Sequential Predictors for Delay-Compensating Feedback Stabilization of Bilinear Systems with uncertainties, "Systems and Control Letters, 152(104933), 9pp., 2021.

This collection of equations includes copies of the original system running on multiple time scales, with additional stabilizing terms, making it possible to compensate for arbitrarily long input delays without having any distributed terms in the controls. However, these results required that the right sides of the systems grow linearly in the input and state, which excludes bilinear systems having the form

$$\dot{x}(t) = A(t)x(t) + \sum_{i=1}^{c} u_i(t-h)(B_i(t)x(t) + G_i(t)) + D(t)\delta(t) \quad (1)$$

with unknown measurable locally essentially bounded functions δ (representing uncertainty), constant delays h, controls $(u = u_1, \ldots, u_c)$, and bounded coefficient matrices. Although such systems are often stabilizable using bounded controls, knowing a bound on u is not sufficient to extend previous sequential predictor results to cover bilinear systems (1). This is because the earlier results also need input-to-state stability (or ISS) with respect to measurement uncertainty, and since one must find a bound $\bar{\delta}$ on the supremum of δ using a bound on the measurement uncertainty; see (7), the third part of the proof of Theorem 1, and [31, Assumption 2].

This calls for the innovations of this work, which eliminates the requirement that the right sides grow linearly in the input and state. These innovations are made possible by our significantly different mathematical analysis, as compared to the study of sequential predictors for linear systems. Our key ingredients include (a) our new Lyapunov–Krasovskii functional construction involving novel uses of Young's inequality and (b) a relaxed condition on the measurement uncertainties in the control (in Assumption 1). This overcomes a longstanding obstacle to building sequential predictors for bilinear systems. See Remarks 1–2 for more on the innovations in our work. We provide input delay compensating sequential predictors for bilinear systems having the form (1) with continuous coefficient matrices, including ISS with respect to the δ, which were not

previously available in the literature. We state and prove a general sequential predictor feedback control result in Sections 3–4. Then Section 5 provides sufficient conditions that facilitate checking our assumptions of our general result. In Section 6, we apply our method to a key class of bilinear systems, which we demonstrate using a power system in Section 7.

3.2. Definitions and Notations

Throughout this paper, the dimensions of the Euclidean spaces are arbitrary unless we note otherwise, and we omit arguments of functions when they are clear. The usual Euclidean norm in $\mathbb{R}^n$ and the induced matrix norm are denoted by $|.|$, and $|\phi|_I$ (resp., $|\phi|_\infty$) is the usual essential supremum of a function ϕ over any interval I in its domain (resp., its entire domain). Consider a system of the form

$$\dot{X}(t) = \mathcal{F}(t, X(t), u_{\mathcal{F}}(t-h), \Delta(t)) \tag{2}$$

whose state X, feedback control $u_{\mathcal{F}}$, and unknown Lebesgue measurable locally essentially bounded function Δ are valued in $\mathbb{R}^{n_2}$, and $\mathbb{R}^{n_3}$, respectively, where $h > 0$ is a constant delay. Owing to the delay, the solutions of (2) are defined for given initial times $t_0 \geq 0$, initial functions that are defined on an initial interval $I^0 \subseteq (-\infty, t_0]$ such as $[t_0 - h, t_0]$, and functions Δ. We assume that (2) is forward complete, i.e., all such solutions are uniquely defined on $I^0 \cup [t_0, \infty)$; see Section 3 for our assumptions that ensure this forward completeness property. We use the well-known standard classes $\mathcal{K}_\mathcal{L}$ and $\mathcal{K}_\infty$of comparison functions from [48, Chapter. 4] and the definition of input-to-state stability (or ISS, which we also use to mean input-to-state stable) for (2); see [49] and [29] for ISS under delays. We use this definition:

3.2.1. Definition 1

Definition 1. For a fixed $u_{\mathcal{F}}$, we say that (2) is ISS with respect to a disturbance set $D \subseteq \mathbb{R}^{n_3}$ provided there are functions $\beta \in \mathcal{K}_\mathcal{L}$ and $\gamma \in \mathcal{K}_\infty$such that for all initial times t_0, initial functions,

and choices of the functions Δ that are valued in D, the corresponding solutions of (2) all satisfy $|X(t)| \leq \beta(|X|_{I^0}, t - t_0) + \gamma\left(\Delta_{[t_0,t]}\right)$ for all $t \geq t_0$.

Let $\mathbb{N} = \{1,2,\dots\}$, and $\mathcal{B}_R$ denote the closed ball of any radius $R > 0$ in Euclidean space centered at the origin. For subsets S_1 and S_2 of Euclidean spaces, a function $W: S_1 \times S_2 \to \mathbb{R}^n$ is called locally Lipschitz in its second variable uniformly in its first variable provided: for each constant $R > 0$, there is a constant $L_R > 0$ such that $|W(s_1, s_a) - W(s_1, s_b)| \leq L_R|s_a - s_b|$ for all $s_1 \in S_1$ and all s_a and s_b in $\mathcal{B}_R$. If L_R in the preceding property can be chosen independently of R, then we use the term globally (instead of locally) Lipschitz. We call a $J: [0,\infty) \times \mathbb{R}^n \to [0,\infty)$ uniformly proper and positive definite provided there exist functions $\gamma \in \mathcal{K}_\infty$ and $\bar{\gamma} \in \mathcal{K}_\infty$ such that $\gamma(|x|) \leq J(t,x) \leq \bar{\gamma}(|x|)$ for all $t \geq 0$ and $x \in \mathbb{R}^n$. We set $\Psi_t(s) = \Psi(t+s)$ for all $\Psi, s \leq 0$, and $t \geq 0$ such that $t + s$ lies in the domain of Ψ. We also use $0_{\ell \times r}$ (resp., I_r) to mean the $\ell \times r$ matrix whose entries are all 0 (resp., the $r \times r$ identity matrix).

3.3. General Result

Before turning to our results on bilinear systems, we provide a novel result for a more general class of systems

$$\dot{x}(t) = f(t, x(t), u(t-h), \delta(t)) \tag{3}$$

whose state x, control u, and unknown Lebesgue measurable locally essentially bounded function δ are valued in $\mathbb{R}^n$, $\mathbb{R}^c$, and $\mathbb{R}^d$ respectively, and $h > 0$ is a constant delay, where we use different notation from (2) in part because the Δ in (2) will not coincide with δ in (3) in Assumption 1 to follow. One difference between the result of this section and [29. Theorem 1] is that here we remove the requirement that the dynamics grow linearly in (x, u), and instead use boundedness conditions on u_3, on the control set, and on the disturbances ϵ and δ; see Remarks 1-2 for more on

the significant differences between this work and [29] and about the value added by this work. We assume:

3.3.1. Assumption 1

There are a compact neighborhood $U \subseteq \mathbb{R}^c$ of $0_{\epsilon\times 1}$, a continuous function $U_s\colon [0,\infty)\times\mathbb{R}^n \to U$ that is globally Lipschitz in its second variable uniformly in its first variable, and a constant $\bar{\epsilon} > 0$ such that the system

$$\dot{x}(t) = f(t, x(t), u_s(t, x(t) + \epsilon(t)), \delta(t)) \tag{4}$$

with disturbance $\Delta = (\epsilon, \delta)$ is ISS with respect to the disturbance set $\mathcal{B}_{\bar{\epsilon}} \times \mathbb{R}^d$. Also, $u_s(t, 0_{n\times 1}) = 0_{c\times 1}$ for all $t \in \mathbb{R}$.

3.3.2. Assumption 2

The function f is continuous, and is locally Lipschitz in (x, u, δ) uniformly in t, satisfies $f(t, 0_{n\times 1}, 0_{cx1}, 0_{d\times 1}) = 0_{n\times 1}$ for all $t \geqslant 0$, and admits a constant $k > 0$ such that

$$|f(t, z_1, U, \Delta_1) - f(t, z_2, U, \Delta_2)| \leq k|z_1 - z_2| + k|\Delta_1 - \Delta_2| \tag{5}$$

holds for all $t \geq 0, z_1 \in \mathbb{R}^n, z_2 \in \mathbb{R}^n, U \in \mathcal{U}, \Delta_1 \in \mathbb{R}^d$, and $\Delta_2 \in \mathbb{R}^d$ for the choice of $\mathcal{U}$ from Assumption 1.

Throughout this paper, we consider any constants $m \in \mathbb{N}$, $\epsilon_* > 0, h > 0, C_1 \in (0, 2m/h), C_2 > 0$, and $\lambda_a > 0$, and any k and $\bar{\epsilon}$ satisfying Assumptions 1-2, and then we set

$$p = \frac{m(4k+\lambda_a)}{2m - hc_1}, \epsilon_{0,\ell} = \max\left\{1, \frac{\bar{C}(1+\lambda_a)h)}{m}\right\}.$$

$$\bar{c} = \frac{p}{C_1}\max\left\{p^2(1+C_2), k^2\left(1+\frac{1}{C_2}\right)\left(1+\frac{\lambda_a}{4}\right)\right\},$$

$$\epsilon_0 = \min\left\{2k\left(1 - \frac{h\bar{C}}{km}(1+\lambda_a)\right), \frac{\bar{C}\lambda_a m}{2(h\bar{C}(1+\lambda_a)+m)}\right\}.$$

$$\hat{c} = \max\left\{\frac{2p^2}{\epsilon_0}, \left(1+\frac{1}{c_2}\right)\frac{p^3}{2C_1}\lambda_a^{\#}, \frac{\epsilon_0}{2}\right\},$$

$$\bar{M} = \frac{k^2}{2\lambda_a} + \lambda_a^{\#}\frac{phk^2}{2c_1 m}\left(1+\frac{1}{C_2}\right), \lambda_a^{\#} = 1 + \frac{4}{\lambda_a}.$$

$$\omega_0 = 1, \omega_i = \frac{2}{\epsilon_0}(\hat{c}\omega_{i-1} + \epsilon_*) \text{ if } 1 \le i \le m-1, \text{ and}$$

$$\bar{\epsilon_*} = \frac{1}{\epsilon_{0,\ell}} m \ \left\{0.5\epsilon_0, \frac{\epsilon_*}{\omega_m - 1}\right\} \tag{6}$$

which will all be positive constants under condition (8) of our theorem. The integer m will serve as the number of sequential predictors, and the constants C_i will serve as weighting functions in our Young's inequality applications in our Appendix. In terms of (6) and any constant

$$\bar{\delta} \in \left(0, \frac{\bar{\epsilon}}{m}\sqrt{\frac{\bar{\epsilon}_*}{2\bar{M}\omega_{m-1}}}\right) \tag{7}$$

(which will serve as our bound on δ) and the function $f_0(t,x,u) = f(t,x,u,0)$, we prove:

3.3.3. Theorem 1

Let $k > 0$ and $\bar{\epsilon} > 0$ be constants such that (3) satisfies Assumptions 1-2. Assume that

$$m > \frac{h\bar{C}(1+\lambda_a)}{k} \tag{8}$$

Consider (3) in closed loop with

$$u(t) = u_s(t+h, z_m(t)) \tag{9}$$

where i_m is the last n components of the state of the system

$$\begin{cases} \dot{z}_1(t) = & f_0\left(t+\frac{h}{m}, z_1(t), \Phi[t, z_m, 1)\right] \\ & -p\left[z_1\left(t-\frac{h}{m}\right) - x(t)\right] \\ \dot{z}_2(t) = & f_0\left(t+\frac{2h}{m}, z_2(t), \Phi(t, z_m, 2)\right) \\ & -p\left[z_2\left(t-\frac{h}{m}\right) - z_1(t)\right] \\ & \vdots \\ \dot{z}_m[t) = & f_0\big(t+h, z_m(t), \Phi(t, z_m, m)\big) \\ & -p\left[z_m\left(t-\frac{k}{m}\right) - z_{m-1}(t)\right] \end{cases} \tag{10}$$

where

$\Phi(t, z_m, i) = u_{,}(t + h - M(m-i)/m, z_m(t - K(m-i)/m))$

for all $t \geq 0$ and $i \in \{1,2, \ldots . m\}$ and $z_0 = x$. Then there are functions $\beta \in \mathcal{K}_{\mathcal{L}}$ and $\gamma \in \mathcal{K}_{\infty}$ such that all solutions $(x, z) : [b_0 - 2h, \infty) \to \mathbb{R}^{(m+1)n}$ of the preceding closed loop system, for all Lebesgue measurable essentially bounded functions δ: $[0, \infty) \to \mathcal{B}_{\overline{\delta}}$ and all initial times $t_0 \geq h/m$, satisfy

$$|x(t)| \leq \beta_d\left(|x|_{\left[t_0-2h, t_0+{}^{h}/_{m}\right]} + |z|_{\left[t_0-2h, t_0+{}^{h}/_{m}\right]}, t - t_0\right) + \gamma_d\big(|\, \delta_{1|_{0,}+1}\big) \tag{11}$$

for all $t \geq t_0$, where $z = (z_1, \ldots, z_m)$

3.3.4. Remark 1

Theorem 1 states that it is possible to design a sequence of m predictors such that, when the un-delayed closed loop system (4) is LS with respect to the disturbance $\delta(t)$ and the uncertainties $\epsilon(t)$ in the state measurements under the bounds on these functions from Assumption 1, then in the presence of delay. The state of the closed loop system with the predictor remains in a ball whose radius depends on the initial conditions and the bound on $\delta(t)$.

It is tempting to surmise that at least in bilinear cases, we can reduce our analysis of (3) to systems that are globally Lipschitz in the state (which were covered in [29], by replacing f by the new dynamics f_{ruw} that is defined by

$$f_{new}(t,x,u,\delta) = \begin{cases} f(t,x,u,\delta), & \text{if } |u| \leq R \\ f(t,x,uR/|u|,\delta), & \text{if } |u| > R \end{cases} \tag{12}$$

for a bound R on the control u_s. However, this replacement would not address the problems in this work, where there is a restriction on the allowable measurement uncertainties ϵ in Assumption 1 (which makes our assumption less restrictive than in [29], where the ISS assumption is required for all choices of the measurement uncertainties $\epsilon(t)$) and where we must therefore find a bound $\bar{s}$ on the allowable uncertainties δ.

Our (less restrictive) condition in Assumption 1 that ϵ remains in a bounded set is called for in order to produce a theorem whose assumptions we can check for bilinear systems; see Lemmas $2-3$. However, the price to pay for only considering ϵ's that stay in a bounded set in Assumption 1 is that it calls for the third part of our proof of our theorem; see especially (32) and (35). The requirement that u_a is valued in the compact set u is used to ensure that (5) is satisfied when U is a control value; see (A.3)-(A.4). The bound on U in Assumption 2 is needed for the existence of the required k when (2) is bilinear; see (41).

3.3.5. Remark 2

Theorem 1 is also new even when $\delta = 0$, because of its less restrictive condition on the number m of sequential predictors, as compared with the condition

$$m > h(4k + \lambda_a)^{3/2}\sqrt{(2/k)(1+\lambda_a)} \tag{13}$$

from [3]; see Section 7. Our strategy for obtaining our less restrictive lower bound (8) on m is to use the degrees of freedom in the Lyapunov-Krasovskii analysis in the Appendix, where the constants C_1 and C_2 arise from using Young's inequality instead of the triangle inequality. This leads to a different Lyapunov-Krasovskii functional in our analysis and a different p in the sequential predictors, as compared with [31], which used $p = 4k + \lambda_a$. Therefore, although the sequential predictors (10) have the same general structure as earlier sequential predictor designs (consisting of copies of the original system running on different time scales with additional corrective terms), there is considerable novelty in our proof that makes it possible to apply this general structure in our novel setting that includes bilinear systems.

A significant difference between works such as [50] and Theorem 1 is that our theorem yields a control having no distributed terms, based on the computationally cheap sequential predictors (10). While Lyapunov methods can produce conservativeness, we believe that this is the price to pay to compensate for arbitrarily long input delays without using distributed terms that would otherwise have occurred from using standard predictive methods while also handling bilinearities. We can provide a global exponential ISS estimate for the error vector (14) (in (30)). which we can combine with (11) to obtain ISS estimates for the combined variable (x, z), where $z = (z_1, \dots, z_m)$ is the vector of predictors (using the fact that $z_i(t) = \varepsilon_i(t) + \varepsilon_{i-1}(t + h/m) + \cdots + \varepsilon_1(t + (i - 1)h/m) + x(t + ih/m)$ for all $t \geq 0$ and $i \geq 2$). We leave the formulas for comparison functions in the ISS estimate for (x, z) to the reader.

3.3.6. Remark 3

Like in [29], our requirement $t_0 \geq h/m$ in Theorem 1 is used in our Lyapunov-Krasovskii analysis but can be relaxed. While the main result of Mazenc and Malisoff [29] contains suprema over $[t_0 - h, t_0 + h/m]$ on the right side of (11) instead of $[t_0 - 2h, t_0 + h/m]$, we use $2h$ instead

of h to allow the special case where $m = 1$. Moreover, we can use the method from [31, Section V] (with its requirement $U \in \mathbb{R}^c$ replaced by $U \in \mathcal{U}$) to replace $[t_0 - 2h, t_0 + h/m]$ by $[t_0 - 2h, t_0]$ in the final estimate (11).

3.4. Proof of Theorem

Throughout the proof, all inequalities and equalities should be understood to hold for all $t \geq t_0$ and $t_0 \geq h/m$ along all solutions of the closed loop system from the statement of the theorem, unless otherwise indicated. Recalling our definition $z_0 = x$, we use the error variables

$\mathcal{E} = (\varepsilon_1, \dots, \varepsilon_{\mathrm{m}})$, where

$$\varepsilon_i(t) = z_i(t) - z_{i-1}(t + h/m) \text{ for } i = 1, \dots, m \tag{14}$$

The rest of the proof has three parts.

First Part: Lyapunov-Krasovskii Functionals for ε_i. We use

$$\hat{\mu}(\varepsilon_{i,t}) = \tfrac{1}{2}|\varepsilon_i(t)|^2 + \int_{t-2\mathrm{h}/m}^{t} |\varepsilon_i(\ell)|^2 \, \mathrm{d}\ell \tag{15}$$

for $i = 1,2, \dots, m$ and the following lemma (which we prove in the Appendix, and where $\varepsilon_{i,t}$ is the ith component of ε_{t} for each i):

3.4.1 Lemma 1

Consider the functions $v(\varepsilon_i) = \frac{1}{2}|\varepsilon_i|^2$ and

$$\mu(\varepsilon_{i,t}) = v(\varepsilon_i(t)) + \bar{C}(1 + \lambda_a) \int_{t-2h/m}^{t} \int_{s}^{\mathrm{t}} v(\varepsilon_i(\ell))\mathrm{d}\ell \mathrm{d}s \text{ and}$$

$$\bar{\mu}(\varepsilon_{i,t}) = \mu(\varepsilon_{i,t}) + \int_{t-2a/m}^{\mathrm{t}} |\mathcal{E}_i(\ell)|^2 \, \mathrm{d}\ell \tag{16}$$

for $i = 1,2, \dots, m$. Then, the inequalities

$$\dot{\mu}(\varepsilon_{1,t}) \leq -\epsilon_0 \tilde{\mu}(\varepsilon_{1,t}) + \bar{M}|\delta|^2_{[t,t+\mathrm{h/m}]}, \tag{17}$$

$$\dot{\mu}(\varepsilon_{1,t}) \leq -\frac{\epsilon_0}{2}\tilde{\mu}(\epsilon_{i,t}) + \frac{p^2}{\epsilon_0}|\varepsilon_{i-1}|^2 + \left(1+\frac{1}{C_2}\right)\frac{p^3}{2C_1}{\lambda_a}^{\#}\int_{t-h/m}^{t}|\varepsilon_{i-1}(\ell)|^2\,\mathrm{d}\ell \tag{18}$$

hold for all $t \geq h/m$ and $i \in \{2, \dots, m\}$.

The proof that ϵ_0 from (6) satisfies the requirements from Lemma 1 uses the fact that the constant $\epsilon_{0,\ell}$ from (6) is such that

$$\begin{aligned}\mu(\varepsilon_{i,t}) \leq\ & \tfrac{1}{2}|\varepsilon_i(t)|^2 \\ & +\bar{C}(1+\lambda_a)\tfrac{2h}{m}\tfrac{1}{2}\textstyle\int_{\mathrm{t}-2h/m}^{t}|\varepsilon_i(\ell)|^2\,\mathrm{d}\ell \\ \leq\ & \epsilon_{0,i}\hat{\mu}(\varepsilon_{i,t})\end{aligned} \tag{19}$$

for $i = 1, \dots, m$ and all $t \geq h/m$. We also use (19) later in the proof below. From our choices (6) of our constants, it follows from Lemma 1 that for all $i \in \{2, \dots, m\}$ and $t \geq h/m$, we have

$$\dot{\mu}(\varepsilon_{i,t}) \leq -\tfrac{\epsilon_0}{2}\hat{\mu}(\varepsilon_{i,t}) + \hat{c}\hat{\mu}(\varepsilon_{i-1,t}). \tag{20}$$

Second Part: ISS Estimate for ε Dynamics. We next show that with the constants ω_i from (6), the function

$$\mu^{\sharp}_{\mathrm{m}}(\varepsilon_{\mathrm{t}}) = \textstyle\sum_{j=1}^{m}\ \omega_{m-j}\mu(\varepsilon_{j,t}). \tag{21}$$

is an ISS Lyapunov-Krasovskii functional for the ε dynamics with the disturbance δ. We use induction and the partial sums.

$$\mu^{\sharp}_{r}(\mathcal{E}_{\mathrm{t}}) = \mu(\mathcal{E}_{\mathrm{m,t}}) + \omega_1\mu(\varepsilon_{\mathrm{m}-1,t}) + \cdots + \omega_r\mu(\mathcal{E}_{\mathrm{m}-r,t}) \tag{22}$$

for $r = 1, \dots, m-1$ when $m \geq 2$. Using the fact that

$$\mu_r^{\sharp}(\mathcal{E}_{\mathrm{t}}) = \mu\big(\mathcal{E}_{\mathrm{m,t}}\big) + (2/\epsilon_0)(\hat{c} + \epsilon_*)\mu\big(\varepsilon_{m-1,t}\big) \tag{23}$$

and (20), we get

$$\dot{\mu}_1^{\#} \leq -\frac{\epsilon_0}{2}\hat{\mu}\big(\varepsilon_{\mathrm{m},t}\big) - \epsilon_*\hat{\mu}\big(\varepsilon_{\mathrm{m}-1,t}\big) + \hat{c}\,\frac{2}{\epsilon_0}(\hat{c} + \epsilon_*)\hat{\mu}\big(\varepsilon_{\mathrm{m}-2,t}\big) \tag{24}$$

holds if $m > 2$ and $t \geq h/m$. On the other hand, for $m = 2$, we can use (17) to verify that

$$\dot{\mu}_1^{\#} \leq -\frac{\epsilon_0}{2}\hat{\mu}\big(\varepsilon_{2,t}\big) - \epsilon_*\hat{\mu}\big(\varepsilon_{1,t}\big) + \frac{2}{\epsilon_0}(\hat{c} + \epsilon_*)\bar{M}|\delta|^2_{[t,t+h/m]} \tag{25}$$

for all $t \geq h/m$. By induction, it follows that.

$$\dot{\mu}_{\mathrm{m}}^{\#} \leq -\frac{\epsilon_0}{2}\hat{\mu}\big(\varepsilon_{\mathrm{m},t}\big) - \epsilon_*\sum_{j=1}^{m-1}\hat{\mu}\big(\varepsilon_{m-j,t}\big) + \omega_{\mathrm{m}-1}\bar{M}|\delta|^2_{[t,t+h/m]} \tag{26}$$

for all $t \geq h/m$ and $m > 1$. Moreover, (19) gives.

$$\omega_{\mathrm{mi}-i}\mu\big(\varepsilon_{\mathrm{i},t}\big) \leq \epsilon_{0,\ell}\omega_{\mathrm{m}-\mathrm{i}-\mu}\hat{\mu}\big(\varepsilon_{\mathrm{i},t}\big) \tag{27}$$

for $i = 1, \ldots, m$ and all $t \geq h/m$, and $1 \leq \omega_i \leq \omega_{i+1}$ for $i = 0, \ldots, m-2$ and $m \geq 2$, since $\hat{c} \geq \epsilon_0/2$. It follows from (19) and (26) and our choice of $\bar{\epsilon}_*$ in (6) that we have

$$\dot{\mu}_{\mathrm{m}}^{\#} \leq -\bar{\epsilon}_*\mu_{\mathrm{m}}^{\#}(\varepsilon_{\mathrm{t}}) + \omega_{\mathrm{m}-1}\bar{M}|\delta|^2_{[t,t+\mathrm{h/m}]} \tag{28}$$

for all $t \geq h/m$. Applying the method of variation of parameters to (28) (by multiplying it through by $e^{\bar{\epsilon}_* t}$ and integrating the result on $[t_0, t]$ for any $t_0 \geq h/m$), we obtain a constant $c_a > 0$ such that

$$\frac{1}{2}|\mathcal{E}(t)|^2 \leq \mu_{\mathrm{m}}^{\#}(\varepsilon_{\mathrm{t}}) \leq c_a e^{\bar{\epsilon}_*(t_0 - t)}|\varepsilon|^2_{[t_0-2\mathrm{h,t}]} + \frac{\omega_{m-1}\bar{M},\delta|^2_{[t_0,t+h/m]}}{\bar{\epsilon}_*} \tag{29}$$

for all $t \geq t_0$. By multiplying (29) through by 2 and using the subadditivity of the square root (to upper bound the square root of the two right side terms), it follows that

$$|\varepsilon(t)| \leq e^{0.5\bar{\epsilon}_*(t_0-t)}\sqrt{2c_a}|\varepsilon|_{[t_0-2h,t_0]} + \sqrt{\frac{2\omega_{m-1}\bar{M}}{\bar{\epsilon}_*}}|\delta|_{[t_0,t+h/m]} \tag{30}$$

holds for the $\mathcal{E}$ dynamics for all $t \geq t_0$ and $t_0 \geq h/m$.

Third part: ISS-Like Estimate for Closed Loop x Dynamics. We show how our new variable.

$$\varepsilon^{\#}(t) = \sum_{\ell=0}^{m-1} \varepsilon_{m-\ell}\left(t + \ell\frac{h}{m} - h\right) \tag{31}$$

can be viewed as a measurement error added to the state $x(t)$ in the feedback control in the closed loop system from the statement of our theorem, which will allow us to apply Assumption 1 with $\epsilon = \varepsilon^{\#}$

To this end, we first choose a constant $\lambda_* \in (0,1)$ that satisfies.

$$\bar{\delta} = \lambda_*\frac{\bar{\epsilon}}{m}\sqrt{\frac{\bar{\epsilon}_*}{2\omega_{n-1}\bar{M}}}, \tag{32}$$

which exists by (7). Since $1/\lambda_* > 1$, the exponential ISS condition in (30) then yields a constant $\mathcal{T} > 0$ such that.

$$|\mathcal{E}(t)| \leq \frac{1}{\lambda_*}\sqrt{\frac{2\omega_{m-1}\bar{M}}{\epsilon_*}}\bar{\delta} \tag{33}$$

for all $t \geq t_0 + \mathcal{g}_\delta$ and such that we also have

$$|\varepsilon^{\#}(t)| \leq m|\varepsilon|_{[t-h,t-h/m]} \leq \frac{m}{\lambda_*}\sqrt{\frac{2\omega_{m-1}\bar{M}}{\bar{\epsilon}_*}}\bar{\delta} = \bar{\epsilon} \tag{34}$$

for all $t \geq t_0 + h + \mathcal{g}_\delta$, where

$$\mathcal{g}_\delta = \mathcal{T}\big(|\chi|_{[t_0-2h,t_0+h/m]}\big) + |z|_{[t_0-2h,t_0+h/m]}), \tag{35}$$

by (32) and our condition $|\delta|_\infty \leq \bar{\delta}$; a formula for the required constant $\mathcal{T}$ can be deduced from the fact that $\ln(1+r) \leq r$ for all $r \geq 0$.

On the other hand, using the fact that

$$z_m(t) = \varepsilon_m(t) + z_{m-1}(t + h/m),$$

$$z_{\mathrm{m}-1}(t) = \varepsilon_{m-1}(t) + z_{m-2}(t + h/m),$$

.... and $z_1(t) = \varepsilon_1(t) + x\left(t + \frac{k}{m}\right)$ (36)

all hold for all $t \geq 0$, it follows (e.g., by induction on m) that $z_m(t) = \varepsilon^{\#}(t+h) + x(t+h)$. Hence, (3) in closed loop with (9) is

$$\dot{x}(t) = f\big(t, x(t), u_s\big(t, x(t) + \mathcal{E}^{\sharp}(t)\big), \delta(t)\big). \tag{37}$$

Then (34) allows us to use Assumption 1 with $\epsilon = \varepsilon^{\#}$ along all solutions of the closed loop system and all $t \geq t_0 + h + \mathcal{g}_\delta$.

In fact, the last part of the proof of Mazenc and Malisoff [29. Theorem 1] with its initial time t_0 replaced by $t_0^{\#} = t_0 + G_0$ allows us to find functions $\beta_b \in \mathcal{K}_{\mathcal{L}}$ and $\gamma_b \in \mathcal{K}_\infty$ such that, for all solutions of the closed loop system of our theorem, and for all $t \geq t_0^{\#}$ and $t_0 \geq h/m$, we have

$$|x(t)| \leq \beta_b\left(|x^{\#}|_{\left[t_0-2h,t_0^{\#}+\frac{h}{m}\right]}, t - t_0 - G_0\right) + \gamma_b\big(|\delta|_{[t_0,t]}\big), \tag{38}$$

where $G_0 = \mathcal{g}_\delta + h$ and $x^{\#} = (x, z)$. On the other hand, Assumptions 1-2 provide a constant $\bar{L} >$

0 (that is independent of the initial condition) such that $|\dot{x}^{\#}(t)| \leq \bar{L}\big(|x^{\#}|_{[t-h,t]} + |\delta|_{[t_0,t]}\big)$ when $t \geq t_0 \geq 0$. Integrating the preceding bound for $|\dot{x}^{\#}(t)|$, and applying Gronwall's inequality to the function $|x^{\#}|_{[t-h,t]}$, we get a constant $c_b > 0$ (which is also independent of the initial condition) so that

$$|x^{\#}(t)| \leq |x^{\#}|_{[t-h,t]} \leq e^{c_b \mathcal{G}_\delta} c_b \hat{G}_0 \big(|x^{\#}|_{[t_0-h,t_0]} + |\delta|_{[t_0,t]}\big) \leq e^{c_b \mathcal{G}_\delta} c_b \big(\hat{G}_0 |x^{\#}|_{[t_0-h,t_0]} + \bar{\delta}\mathcal{G}_\delta + 2h|\delta|_{[t_0,t]}\big) \leq \mathcal{M}\big(|x^{\#}|_{(t_0-2h,t_0+h/m]}\big) + \mathcal{L}\big(|\delta|_{[t_0,t]}\big) \quad (39)$$

for $t \in [t_0, t_0^{\#} + h/m]$, with $\hat{G}_0 = \mathcal{G}_\delta + 2h, M(s) = 2c_b s e^{2c_b \mathcal{T} s}\Big(\mathcal{T}\big(s + \bar{\delta}\big) + 2h\big(1 + \bar{\delta} c_b \mathcal{T}\big)\Big)$, and where $\mathcal{L}(s) = 2c_b h s$, and where we used

$2hc_b e^{2c_b \mathcal{T} s}|\delta|_{[t_0,t]} \leq 2hc_b(c_b \mathcal{T} s e^{2c_b \mathcal{T} s} + 1)|\delta|_{[t_0,t]} \leq 2\bar{\delta} h {c_b}^2 \mathcal{T} e^{2c_b \mathcal{T} s} s + 2hc_b|\delta|_{[t_0,t]}$ (which is a consequence of the bound $e^r \leq re^r + 1$ for $r \geq 0$) and

$$|x|_{[t_0-2h,t_0+h/m]} + |z|_{[t_0-2h,t_0+h/m]} \leq 2|x^{\#}|_{[t_0-2h,t_0+h/m]} \quad (40)$$

and $|\delta|_\infty \leq \bar{\delta}$. Using (39) to upper bound the first argument of β_b in (38), and then using the fact that $\beta_b(r_1 + r_2, r_3) \leq \beta_b(2r_1, r_3) + \beta_0(2r_2, 0)$ for all nonnegative r_1, r_2, and r_3, it follows that we can upper bound the first right side term of (38) by

$\beta_b\big(M^{\#}\big(|x^{\#}|_{[t_0-2h,t_0+h/m]}\big), t - t_0^{\#}\big) + \beta_b\big(2\mathcal{L}\big(|\delta|_{(t_0,t]}\big), 0\big)$ with $M^{\#}(s) = \max\{s, 2M(s)\}$. Hence, by separately considering times $t \in [t_0, t_0^{\#}]$ and $t > t_0^{\#}$. We conclude that we can satisfy the requirements of Theorem 1 with

$\beta_d(s,t) = \max\big\{\mathcal{M}(s)e^{2\mathcal{T}s + h - t}, \beta_b(M^{\#}(s), \max\{t - 2\mathcal{T}s - h, 0\})\big\}$ and

$\gamma_d(s) = \max\{\mathcal{L}(s), \beta_b(2\mathcal{L}(s), 0) + \gamma_b(s)\}$.

3.5. Checking our Assumption

The growth requirement (5) from Assumption 2 holds for our bilinear systems (1) for any bounded neighborhood $\mathcal{U} \subseteq \mathbb{R}^c$ of the origin and any bounded continuous functions A, D, B_i, and G_i for each i. This follows by picking

$$k = \max\{|A|_\infty + \bar{U} \sum_{i=1}^{c} |B_i|_\infty, |D|_\infty\} \tag{41}$$

for any bound $\bar{U}$ on the elements of $\mathcal{U}$. However, it is less trivial to check Assumption 1, so we next present sufficient conditions for Assumptions 1-2 to hold for some u_s. We specialize the sufficient conditions from this section to bilinear systems in the next section. We prove the following, whose condition (a) differs from a standard Lyapunov decay condition because α_0 is not required to be positive definite:

3.5.1. Lemma 2

Let f in (3) admit a compact neighborhood $\mathcal{U} \subseteq \mathbb{R}^c$ of the origin and a constant $k > 0$ such that the requirements from Assimption 2 hold. Let $\bar{\omega} > 0$ be a constant such that $[-\bar{\omega}, \bar{\omega}]^c \subseteq \mathcal{U}$. Assume that there are a C^1 function $V: \mathbb{R}^{n+1} \to [0, \infty)$, a continuous $\alpha_0: \mathbb{R}^n \to [0, \infty)$, a function $\gamma_* \in \mathcal{K}_\infty$, and C^1 functions $M_i: \mathbb{R} \times \mathbb{R}^n \to \mathbb{R}$ that are locally Lipschitz in the second variable uniformly in the first variable for $i = 1, 2, \ldots, c$ such that:

(a) the inequality,

$$\dot{V} \leq -\alpha_0(x(t)) + \sum_{i=1}^{c} u_1 M_i(t, x(t)) + \gamma_*(|\delta(t)|) \tag{42}$$

holds along all solutions of $\dot{x}(t) = f(t, x(t), u, \delta(t))$ for all $t \geq 0$ and each vector $u \in U$;

(b) the functions,

$$\alpha_0(x) + \sum_{i=1}^{c} |M_i(t, x)| \text{ and } V(t, x) \tag{43}$$

are uniformly proper and positive definite; and

(c) the functions, $M_i^*(t,x) = (\partial M_i / \partial x)(t,x)/(1 + M_i^2(t,x))$ are bounded on $\mathbb{R}^{n+1}$ for $i = 1, \dots, c$. Choose any positive value

$$\bar{L}_* \geq \sup\{|M_i^*(t,x)| : (t,x) \in \mathbb{R}^{n+1}, 1 \leq i \leq c\}. \tag{44}$$

Then Assumption 1 is satisfied for any constant

$$\bar{\epsilon} \in \left(0, \frac{\pi}{2\bar{L}_*}\right) \tag{45}$$

and $u_s = -\frac{2\bar{\omega}}{\pi}\big(\arctan(M_1), \dots, \arctan(M_i)\big)$.

3.5.2. Proof

For each tuple $(t,x) \in \mathbb{R} \times \mathbb{R}^n$, each $\epsilon \in \mathbb{R}^n$, and each $i \in \{1,2,\dots,c\}$, we can apply the Fundamental Theorem of Calculus to the function

$$\mathcal{M}_i^{t,x\epsilon}(\lambda) = \arctan(M_i(t, x + \lambda\epsilon)) \tag{46}$$

on the interval $[0,1]$ to verify that

$$|\arctan(M_i(t,x+\epsilon)) - \arctan(M_i(t,x))| = \left|M_i^{t,x,\epsilon}(1) - M_i^{t,x,\epsilon}(0)\right| \leq \int_0^1 \left|\dot{M}_i^{t,x,\epsilon}(s)\right| ds =$$

$$\int_0^1 |M_i^*(t, x + s\epsilon)\epsilon| ds \leq \bar{L}_*|\epsilon| \tag{47}$$

and so also

$$-\arctan(M_i(t,x+\epsilon)M_i(t,x) \leq -\arctan(M_{\mathrm{i}}(t,x))M_{\mathrm{i}}(t,x) + \bar{L}_*|\epsilon||M_1(t,x)| \tag{48}$$

Fixing constants $w_* > 0$ and $\delta_* \in (0,1)$ such that $\bar{\epsilon} = \delta_* \pi/(2\bar{L}_*)$ (which exist by (45)) and such that arctan(s) $\geqslant (\delta_* + 1)\pi/4$ for all $s \geq w_*$ (which exists because $\lim_{s\to+\infty}$ arctan(s) $= \pi/2$) and any $(t,x) \in \mathbb{R}^{n+1}$, $1 \in \{1,2,\ldots,c\}$, and $\epsilon \in \mathcal{B}_{\bar{\epsilon}}$, we consider two cases:

Case 1. $|M_i(t,x)| \leq w_*$. To cover this case, we fix a constant $c_0 > 0$ such that $\arctan(s) \geq c_0 s$ for all $s \in [0, w_*]$. Then we can use the fact that arctan is an odd function to upper bound the right side of (48) by $-c_0 M_i^2(t,x) + \bar{L}_*|\epsilon||M_i(t,x)| \leq -\frac{1}{2}c_0 M_i^2(t,x) + \frac{1}{2c_0}\bar{L}_*{}^2|\epsilon|^2$, where we used Young's inequality $ab \leq c_0 a^2/2 + b^2/(2c_0)$ with $a = |M_i(t,x)|$ and $b = \bar{L}_*|e|$ to upper bound $\bar{L}_*|\epsilon||M_i(t,x)|$.

Case 2. $|M_i(t,x)| > w_*$. In this case, we can use the fact that arctan is nondecreasing on $[0,\infty)$ and odd to upper bound the right side of (48) by $-(\pi/4)(\delta_* + 1)|M_i(t,x)| + \bar{L}_*|\epsilon||M_i(t,x)| \leq -(1-\delta_*)(\pi/4)M_i(t,x)]$, by our choices of δ_*, and w_*.

Combining the previous two cases, we conclude that for all choices of the functions δ and ϵ from Assumption 1, the time derivative of V along all solutions of (4) satisfies

$$\dot{V} \leq -\{\alpha_0(x) + \textstyle\sum_{i=1}^{c} g_i(t,x)\} + \gamma_*(|\delta|) + \frac{\bar{\omega}}{c_0\pi}\bar{L}_*{}^2|\epsilon|^2 \tag{49}$$

where $g_i(t,x) = \frac{2\bar{\omega}}{\pi}\min\left\{(c_0/2)M_i^2(t,x), (1-\delta_*)\frac{\pi}{4}|M_i(t,x)|\right\}$ for each i and $t \geq 0$. Recalling our assumption (b), we conclude that the sum in curly braces in (49) is uniformly proper and positive definite. Therefore, V is an ISS Lyapunov function for this closed loop system (as defined, e.g., in [48, Chapter 4]) for disturbances (ϵ, δ) valued in $\mathcal{B}_{\bar{\epsilon}} \times \mathbb{R}^d$, giving the ISS property of Assumption 1.

3.5.3. Remark 4

We can replace the formulas $\arctan(M_i(t,x))$ in Lemma 2 by $\sigma_i(M_i(t,x))$ for any functions $\sigma_i: \mathbb{R} \to \mathbb{R}$ that satisfy: σ_i is a bounded C^1 strictly increasing odd function, $\lim_{s\to 0} \sigma_i(s)/s > 0$, and $\sigma_i'(M_i(t,x))(\partial M_i/\partial x)(t,x)$ is a bounded function for $i = 1, ...$, c. Then Lemma 2 remains true if we replace $\pi/2$ in (45) by $\max_i |\sigma_i|_\infty$, replace the M_i^* formulas by $M_i^*(t,x) = \sigma_i'(M_i(t,x))(\partial M_i/\partial x)(t,x)$, and replace $2/\pi$ in the u_s formula by $1/\sup_s \sigma_i(s)$, by a similar proof.

3.6. Application to Bilinear Systems

This special case of Lemma 2 covers bilinear systems, and is obtained by specializing Lemma 2 to the case where $M_i(t,x) = 2(x^\top P(t)B_i(t)x + x^\top P(t)G_i(t))$ using a quadratic Lyapunov function $V(t,x) = x^\top P(t)x$:

3.6.1. Lemma 3

Let $A: \mathbb{R} \to \mathbb{R}^{n\times n}, D: \mathbb{R} \to \mathbb{R}^{n\times d}$, and $B_i: \mathbb{R} \to \mathbb{R}^{n\times n}$ and $G_i: \mathbb{R} \to \mathbb{R}^n$ for $i = 1, \ldots, c$ be bounded matrix valued continuous functions. Assume that there are a function $\gamma_* \in \mathcal{K}_\infty$, constants $c_i \geq 0$, and a C^1 bounded function $P: \mathbb{R} \to \mathbb{R}^{n\times n}$ such that $P^\top(t) = P(t)$ for all $t \in \mathbb{R}$ and such that the following hold with $V(t,x) = x^\top P(t)x$:

(a) along all solutions of $\dot{x} = A(t)x + D(t)\delta$, we have

$$\dot{V} \leq -\sum_{i=1}^n c_i x_i^2(t) + \gamma_*(|\delta(t)|) \tag{50}$$

at all times $t \geq 0$;

(b) the functions $V(t,x)$ and

$$\sum_{i=1}^n c_i x_i^2 + \sum_{i=1}^c |x^\top P(t)B_i(t)x + x^\top P(t)G_i(t)| \tag{51}$$

are uniformly proper and positive definite; and

(c) the functions

$$\mathcal{H}_i(t,x) = \frac{2\left(x^T\left(P(t)B_i(t)+B_i{}^T(t)P(t)\right)G_i{}^T(t)P(t)\right)}{1+4(x^TP(t)B_i(t)x+x^TP(t)G_i(t))^2} \tag{52}$$

are bounded for $i = 1, \dots, c$.

Choose a positive value $\mathcal{H}_* \geq \sup\{|\mathcal{H}_{\mathrm{i}}(t,x)|\colon (t,x) \in \mathbb{R}^{n+1}, 1 \leq i \leq \mathrm{c}\}$. Then, for any constants $\bar{\omega} > 0$ and $\bar{\epsilon} \in \left(0, \pi/(2\mathcal{H}_*)\right)$ and with the feedback

$$u_s(t,x) = -\bar{\omega}\left(\arctan\left(M_1(t,x)\right), \dots, \arctan\left(M_c(t,x)\right)\right) \tag{53}$$

where $M_i(t,x) = 2(x^{\top}P(t)B_i(t)x + x^{\top}P(t)G_i(t))$,

the bilinear system (1) satisfies Assumptions 1-2.

The preceding results are novel, even in the special case where the coefficient matrices in (1) are constant. To illustrate Lemma 3 in the constant coefficients case, we consider the case where the coefficient matrices in (1) and P are

$$A = \begin{bmatrix} A_0 & 0_{n_a\times n_b} \\ 0_{n_b\times n_e} & 0_{n_b\times b_b} \end{bmatrix}, P = \begin{bmatrix} P_0 & 0_{n_b\times n_b} \\ 0_{n_b\times n_a} & P_1 \end{bmatrix}, \tag{54}$$

$$D = \begin{bmatrix} D_1 \\ 0_{n_b\times d} \end{bmatrix}, B_i = \begin{bmatrix} B_{i1} & B_{i2} \\ B_{i3} & B_{i4} \end{bmatrix}, \text{ and } G_i = \begin{bmatrix} G_{i1} \\ G_{i2} \end{bmatrix} \tag{55}$$

for $i = 1, \dots, c$ for any n_a and $n_b = n - n_a$, where A_0 is Hurwitz and $P_0 \in \mathbb{R}^{n_a\times n_a}$ and $P_1 \in \mathbb{R}^{n_b\times n_b}$ are symmetric positive definite matrices, and

$$P_0A_0 + A_0^{\top}P_0 = -I_{\mathrm{n}_a} \tag{56}$$

and where the upper sub-matrices in the block matrices D, B_{i}, and G_i consist of n_a rows. Using the triangle inequality, it follows that along all solutions of $\dot{x} = Ax + D\delta$, we have

$$\dot{V} = -|x_a|^2 + 2x_a^{\top} P_0 D_1 \delta \leq -\frac{1}{2}|x_a|^2 + 2|P_0|^2 |D_1|^2 |\delta|^2 \tag{57}$$

where x_a denotes the first n_a components of x. It follows that we can satisfy requirement (a) of Lemma 3 using $c_{\mathrm{i}} = 0.5$ if $1 \leq i \leq n_a$ and $c_i = 0$ if $n_a < i \leq n$ and $\gamma_o(s) = 2|P_0|^2 |D_1|^2 s^2$. Hence, if we let x_b denote the last n_b components of x, then condition (b) of Lemma 3 will also be satisfied provided

$$\mathcal{N}(x_b) = \sum_{i=1}^{c} |x_b^{\top} P_1 B_{i4} x_b + x_b^{\top} P_1 G_{\mathrm{i2}}| \tag{58}$$

is proper and positive definite. This produces the following sufficient condition for condition (b) of Lemma 3 to hold when the coefficient matrices are constant: There is an index $i \in \{1, \ldots, c\}$ such that $P_1 G_{\mathrm{i2}} = 0$ and $P_1 B_{i4}$ such that is either negative definite or positive definite.

3.7. Conclusions

We presented a new sequential predictor approach to feedback stabilization under arbitrarily long constant input delays which can be applied to bilinear systems that violate the usual linear growth conditions. Compared with other delay compensation approaches, potential advantages include that the closed loop systems satisfy ISS without using distributed terms in the control that were present in exact predictor approaches. This work serves as a basis to explore applications to large scale networked systems as in [41] and extensions for reaction–diffusion PDEs as in [42]. We will also study cases where there are different delays in different components of the input, which may call for bilinear analogs of the predictor structures from [30] having different sets of chain predictors corresponding to the different input delays.

Chapter 4. Delay-Compensating Stabilizing Feedback Controller for a Grid-Connected PV/Hybrid Energy Storage System

4.1. Introduction

Power electronic converters (PECs) are the enabling technology for interfacing and integrating renewable energy sources (RESs), such as solar and wind, with the grid. Energy storage systems, such as batteries and supercapacitors (SCs), interfaced with the grid by PECs are promising solutions for addressing the intermittent nature of RESs and ensuring the delivery of constant energy to the grid. Batteries offer higher energy densities, making them suitable for delivering or absorbing energy over long time periods, while SCs offer higher power densities, making them suitable for delivering or absorbing energy over short-time periods. Therefore, a hybrid energy storage system (HESS) comprised of a battery and an SC offers high power and high energy density [2].

In grid-connected PECs, such as three-phase dc/ac inverters and buck/boost dc/dc converters, the control goal is commonly to regulate voltage, current, or power. Analog voltage and current measurements are sent to a digital signal processor (DSP), and after being processed according to the control algorithm, control inputs are generated in the form of switching signals, which are sent to a pulsewidth modulator. Through pulsewidth modulation (PWM), the switching (ON or OFF) states of the PEC's switching devices are then determined. Due to analog-to-digital conversion (ADC) and depending on the computational complexity of the control algorithm, delays will be present in the digital implementation of the PEC's control, which could potentially lead to grid

This chapter was previously published as I. bhogaraju, J. N. Forestieri. M. Malisoff, and M. Farasat, “Delay-Compensating Stabilizing Feedback Controller for a Grid-Connected PV/Hybrid Energy Storage System,” IEEE Transactions on Control Systems Technology.

stability issues because of frequency and voltage deviations [51]. The work [3] studies the delay that is caused in ADC and PWM and its detrimental effect on stability and system performance. Several delay compensating techniques for grid-connected PECs have been proposed. In grid-connected inverters with an inductor-capacitor-inductor (LCL) filter, the inherent resonance in the filter is handled by active damping, which often suffers from control delay problems. Capacitor current feedback methods are commonly used to reduce the computational delays [52], [53], [54]. In [55], delay compensation is achieved by shifting the capacitor current sampling instant toward the PWM reference update instant. In [56], the critical delay time to keep system stable is analyzed, and a delay time control method is proposed. A stability evaluation method based on developing a critical value for the damping coefficient is proposed in [57].

In [58], a multistep model predictive voltage control with delay compensation is proposed for eliminating undesired oscillations and improving output voltage tracking of a neutral point clamped inverter. The work [59] proposes a model predictive control that uses a weighted filter predictor to improve time delay compensation in a single-phase grid-connected voltage-source inverter. A modified model predictive control is proposed in [60] for PECs in a wind power system. A multiple vector model predictive control method is presented in [61], where determining the vector sequence and duration is simplified to reduce the computational complexity of the control algorithm and, thus, reduce the digital implementation delay. The paper [62] proposes a two-step ahead prediction approach to compensate for the adverse effect of such a delay. These papers, however, do not provide proof of stability of their model predictive control techniques. A variation of Smith's predictor is proposed in [63]. However, the need for a precise system model to design the controller is inevitable in standard predictor-based approaches.

In [64], a current observer is designed for compensating for voltage distortion of a voltage-source inverter. However, control performance is compromised due to the conservative optimization method that is used. To improve closed-loop robustness, a proportional-type Luenberger observer is

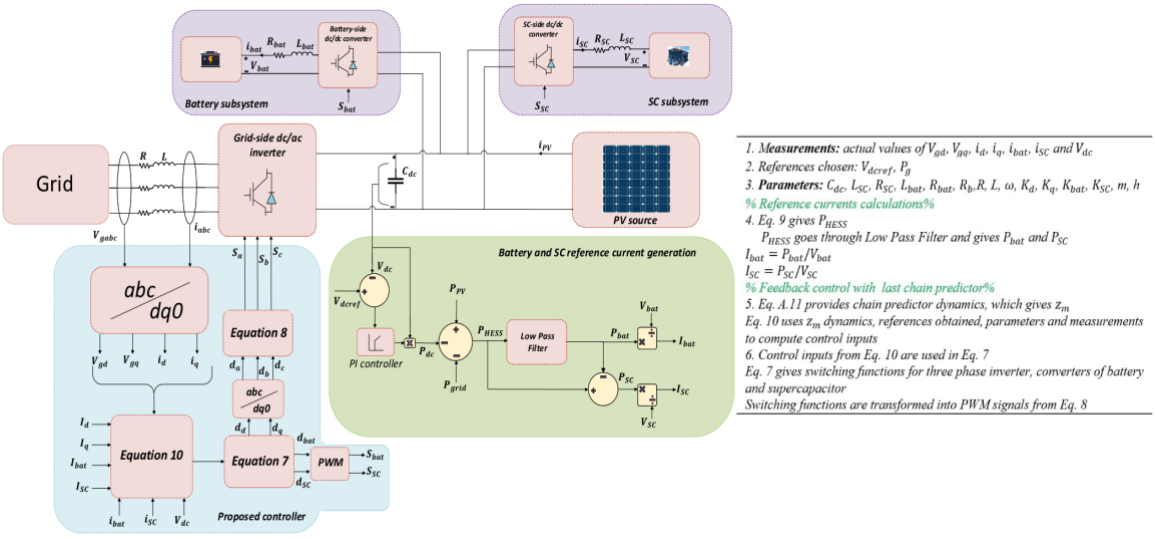

Figure. 4.1. PV/HESS system circuit diagram and control scheme with pseudocode based on (7)–(10) and (A.11).

implemented in [65]. This, however, poses a great challenge in the form of an offset error on the controlled output.

To eliminate these offset errors, full-state proportional-integral observers are used with an adaptation algorithm [66]. A learning algorithm-based control using Luenberger and disturbance observers is proposed in [67]. The disturbance observer resolved the problem of offset errors in steady state, and the learning algorithm alleviated the computational complexity. However, the main drawback of this method is that inaccurate tuning of the parameters can destabilize the overall system performance.

Lyapunov theory is widely used for the stability analysis of nonlinear systems [68]. In [68], upper bounds on the input delays under which an emulation-based control ensures global asymptotic stability are computed using Lyapunov–Krasovskii functionals. The main disadvantage of this method is in its bounds on the allowable delays, which are not suitable for applications with long delays as compared with a system's total response time. The reduction model approach introduced in [69] can compensate for arbitrarily long input delays.

A disadvantage of a standard reduction model or standard prediction-based approaches is that they involve distributed terms, which are undesirable in practical applications. To address this problem, sequential predictors (which are also called chain predictors) were introduced in [29], where the distributed terms are replaced by dynamical extensions that include copies of the original systems running on multiple time scales; see [30], [70], [31], and [32]. The computational challenges caused by distributed terms are, thus, eliminated, while still compensating for arbitrarily long delays. The linear growth condition in [31] and [32] precluded covering bilinear systems. This condition is removed in the work [71] on bilinear systems, where computational time delays that arise in a DSP are compensated for in the case of a grid-connected photovoltaic (PV) system through a three-phase inverter. The power systems examples in these works did not cover the full extent of how energy storage systems are integrated with the PV system and the grid.

Here, we propose a computationally simple delay compensating global asymptotically stabilizing feedback control based on sequential predictors for a grid-connected PV/battery/SC system. As shown in Figure. 4.1, the PV system is interfaced with the grid using a three-phase dc/ac inverter, and the battery and the SC are interfaced with the dc-link capacitor of the inverter, using individual buck/boost dc/dc converters. Due to utilization of PECs, the grid-connected

PV/battery/SC system is prone to time delays. This work handles such delays while maintaining the system's stability.

The major contributions of this brief are threefold.

1) A state-of-the-art delay compensation method for bilinear systems is proposed that features ensured global asymptotic stability in the presence of arbitrary delays and real-time implementation feasibility.

2) Efficacy of the proposed method in compensating for delays due to digital implementation is verified through real-time simulations of a grid-connected PV/battery/SC system.

3) Effectiveness of the proposed method in reducing the computational complexity and the amplitude of the state variables' oscillations is illustrated through comparative real-time simulation studies with a controller designed based on a finite spectrum assignment (FSA) approach.

Also, although we constructed our sequential predictor controller under the assumption of a given delay, we found that our control continues to provide desired convergence to the steady state even if the delay is increased significantly. This illustrates the robustness of our method to the delay value.

This brief is organized as follows. The model for the PV/battery/SC system is in Section II. The procedure to implement the control theory is discussed in Section III. The control theory underlying this implementation is reviewed in the Appendix, which derives required formulas for our controls. Section IV has our real-time simulations and discussions. This brief is concluded in Section V.

4.2. PV/BATTERY/SC SYSTEM MODEL

4.2.1. System Description

The system circuit diagram is shown in Figure. 4.1, where the PV source is modeled as a controlled current source connected to the three-phase inverter via a dc-link capacitor. An L-filter connects the three-phase inverter to the grid. The control signals are the PWM signals for the inverter and both the battery and SC dc/dc converters.

4.2.2. System Dynamics

The dynamics of the system in Figure. 4.1 are expressed as follows:

$$L\frac{di_d}{dt} = d_d V_{\mathrm{dc}} - V_{gd} + \omega L i_q - R i_d$$

$$L\frac{di_q}{dt} = d_q V_{\mathrm{dc}} - V_{gq} - \omega L i_d - R i_q$$

$$C_{\mathrm{dc}}\frac{dV_{\mathrm{dc}}}{dt} = i_{\mathrm{PV}} - d_d i_d - d_q i_q - d_{\mathrm{bat}} i_{\mathrm{bat}} - d_{\mathrm{SC}} i_{\mathrm{SC}}$$

$$L_{\mathrm{bat}}\frac{di_{\mathrm{bat}}}{dt} = d_{\mathrm{bat}} V_{\mathrm{dc}} - R_{\mathrm{bat}} i_{\mathrm{bat}} + V_{\mathrm{bat}}$$

$$L_{\mathrm{SC}}\frac{di_{\mathrm{SC}}}{dt} = d_{\mathrm{SC}} V_{\mathrm{dc}} - R_{\mathrm{SC}} i_{\mathrm{SC}} + V_{\mathrm{SC}} \qquad (1)$$

whose derivation and notation are as follows. The dynamics (1) are obtained using Kirchhoff's voltage and current laws and are expressed in the synchronously rotating *dq*0 reference frame. Park's transformation [50, Appendix 3] is used for converting three-phase quantities into *dq*0 quantities, which are dc. The reference *q*-component of the grid voltage and current as well as the grid reactive power can be set to 0. The battery and SC can be modeled as voltage sources with series resistances for the mathematical analysis. The inverter currents in the *dq*0 frame, dc-link voltage, and battery and SC currents are selected as state variables for control system design.

Here, i_{PV} denotes the current value of the PV source; d_a, d_b, and d_c are inverter switching functions in the *abc* frame and are transformed into d_d and d_q using Park's transformation; V_{ga}, V_{gb}, and V_{gc} are the grid three-phase voltages; V_{gd} and V_{gq} are the *dq* components of the grid voltage; i_a, i_b, and i_c are the grid three-phase currents; i_d and i_q are the *dq* components of the grid current; and d_{bat} and d_{SC} are the duty ratios of the dc/dc converters of the battery and SC, respectively. The constants and variables V_{bat}, V_{SC}, i_{bat}, i_{SC}, and V_{dc} are the battery voltage, SC voltage, battery current, SC current, and dc-link voltage, respectively, and are written using:

$$V_{\text{bat}} = V_{\text{ob}} - i_{\text{bat}}R_b \text{ and } V_{\text{SC}} = V_{\text{os}} - i_{\text{SC}}R_S. \quad (2)$$

Here, V_{ob} and R_b are the internal voltage and resistance of the battery, respectively, and V_{os} and R_S are the internal voltage and resistance of the SC, respectively. The constants L and R are the line resistance and inductance. The known constants L_{bat} and R_{bat} are the battery inductance and resistance, respectively, the known constants L_{SC} and R_{SC} are the SC inductance and resistance, respectively, the known constant C_{dc} is the dc-link capacitance, and the known constant ω is the grid angular frequency. The constants C_{dc}, L_{bat}, R_{bat}, L_{SC}, R_{SC}, i_{PV}, L, R, V_{ob}, V_{os}, and ω are positive, and the constants V_{gd}, V_{gq}, R_b, and R_s are nonnegative.

To specify our stabilization problem, we next represent the steady state model at a time-varying reference solution. These reference state currents and voltages are reference values for the state variable candidates in (1), and so must satisfy

$$L\frac{dI_d}{dt} = D_d V_{\text{dcref}} - V_{gd} + \omega L I_q - R I_d$$

$$L\frac{dI_q}{dt} = D_q V_{\text{dcref}} - V_{gq} - \omega L I_d - R I_q$$

$$C_{\text{dc}}\frac{dV_{\text{dcref}}}{dt} = i_{\text{PV}} - D_d I_d - D_q I_q - D_{\text{bat}} I_{\text{bat}} - D_{\text{SC}} I_{\text{SC}}$$

$$L_{\mathrm{bat}}\frac{dI_{\mathrm{bat}}}{dt} = D_{\mathrm{bat}}V_{\mathrm{dcref}} - R_{\mathrm{bat}}I_{\mathrm{bat}} + V_{\mathrm{bat\_s}}$$

$$L_{\mathrm{SC}}\frac{dI_{\mathrm{SC}}}{dt} = D_{\mathrm{SC}}V_{\mathrm{dcref}} - R_{\mathrm{SC}}I_{\mathrm{SC}} + V_{\mathrm{SC\_s}} \quad (3)$$

where capitalization of letters or subscripts ref or _s indicate the corresponding reference values that correspond to the variables in (1), so, for instance

$$V_{\mathrm{bat\_s}} = V_{\mathrm{ob}} - I_{\mathrm{bat}}R_b \text{ and } V_{\mathrm{SC\_s}} = V_{\mathrm{os}} - I_{\mathrm{SC}}R_S. \quad (4)$$

The errors between the actual measured quantities and their reference values will be our state variables

$$x_1 = i_d - I_d$$

$$x_2 = i_q - I_q$$

$$x_3 = V_{dc} - V_{dcref}$$

$$x_4 = i_{bat} - I_{bat}$$

$$x_5 = i_{SC} - I_{SC} \quad (5)$$

By (1)– (3), we obtain the error dynamic (6)

$$\dot{x}_1(t) = \frac{1}{L}\left[D_d(t)x_3(t) + u_1(t-h)\left(x_3(t) + V_{dcref}(t)\right) - R_1x_1(t) + \omega L x_2(t)\right]$$

$$\dot{x}_2(t) = \frac{1}{L}\left[D_q(t)x_3(t) + u_2(t-h)\left(x_3(t) + V_{dcref}(t)\right) - R_1x_3(t) - \omega L x_1(t)\right]$$

$$\dot{x}_3(t) = \frac{1}{C_{dc}}\big[-D_d(t)x_1(t) - u_1(t-h)(x_1(t) + I_d(t)) - D_q(t)x_2(t) - u_2(t$$
$$- h)\big(x_2(t) + I_q(t)\big) - D_{batt}(t)x_4(t) - u_3(t-h)(x_4(t) + I_{bat}(t))$$
$$- D_{SC}(t)x_5(t) - u_4(t-h)(x_5(t) + I_{SC}(t))\big]$$

$$\dot{x}_4(t) = \tfrac{1}{L_{bat}}\big[D_{bat}(t)x_3(t) + u_3(t-h)\big(x_3(t) + V_{dcref}(t)\big) - R_{bat}x_4(t) + \Delta V_{bat}\big]$$

$$\dot{x}_5(t) = \tfrac{1}{L_{SC}}\big[D_{SC}(t)x_3(t) + u_4(t-h)\big(x_3(t) + V_{dcref}(t)\big) - R_{SC}x_5(t) + \Delta V_{SC}\big] \quad (6)$$

where $\Delta V_{\text{bat}} = V_{\text{bat}} - V_{\text{bat\_s}}$, and $\Delta V_{\text{SC}} = V_{\text{SC}} - V_{\text{SC\_s}}$. In (6), the control inputs are the switching functions for the three-phase inverter in the $dq0$ frame, and the switching states for the battery and SC's dc/dc converters, and are the differences $\Delta d_d, \Delta d_q, \Delta d_{\text{bat}}$, and Δd_{SC} given by

$$u_1 = \Delta d_d = d_d - D_d$$

$$u_2 = \Delta d_q = d_q - D_q$$

$$u_3 = \Delta d_{bat} = d_{bat} - D_{bat}$$

$$u_4 = \Delta d_{SC} = d_{SC} - D_{SC} \quad (7)$$

between the control and reference values, where

$$d_k = S_k - \tfrac{S_a + S_b + S_c}{3}, \text{ for } k = a, b, \text{ and } c$$

$$d_{\text{bat}} \overset{\text{PWM}}{\rightarrow} S_{\text{bat}}, \text{ and } d_{\text{SC}} \overset{\text{PWM}}{\rightarrow} S_{\text{SC}}. \quad (8)$$

The switching states on the right-hand sides of (8) are generated by PWM. The goal is to choose the controls u_i, so that (6) satisfies a global asymptotic stability property (as explained below), to

ensure that the reference trajectory is tracked. Since (6) is bilinear (i.e., its right-hand side has products of state and control components), it is outside the scope of linear control systems.

4.2.3. HESS

The HESS includes a battery and an SC, each with their individual bidirectional dc/dc buck-boost converter. The flow of HESS power, $P_{\text{HESS,}}$, is controlled through the PWM signals that are sent to the dc/dc converters interfacing the battery and SC and is obtained by

$$P_{\text{HESS}} = P_{\text{pv}} - P_{\text{dc}} - P_g \tag{9}$$

where $P_{\text{pv}}, P_{\text{dc}}$, and P_g are the PV, dc link, and grid power, respectively. This relationship follows the power balance principle at the dc link; i.e., the PV power entering the dc link is the sum of the powers delivered to the grid, the HESS, and the dc-link capacitor. It is noteworthy to mention that for proper operation of the dc/ac inverter, the dc-link voltage, V_{dc}, needs to be maintained constant at a reference value. As seen in Figure. 4.1, this is achieved by employing a PI controller and regulating the dc-link power, P_{dc}. The PWM signals are switching states averaged over one time period and defined in (8).

To reduce stress on the battery and lengthen its lifespan, the SC is assigned the role of handling sudden surges and changes, while the battery's role is to provide smooth energy flow over long time periods. To achieve this, P_{HESS} is passed through a low-pass filter (LPF). The low-frequency output component of the LPF is assigned as the reference power that must be supplied/absorbed by the battery, P_{bat} , and the high-frequency component is assigned as the reference power that the SC must supply/absorb, P_{SC}. Once the battery and SC reference powers are determined, the reference battery and SC currents, which are the reference states in (3), are then readily determined

by dividing the reference powers by the corresponding voltages. The pseudocode provided in Figure. 4.1 summarizes the steps to the control system design.

4.3. Controller Design

We show how the computational time delay of our method can be compensated. We design our delay-compensating feedback controller for (6) using a substitute variable in the controls, as follows. Instead of the difference variables x_i, the controls are computed in terms of the last chain predictor in a chain of predictors. The predictors are 5-D dynamic extensions having the state components z_{i_j}, which denotes the j th component of predictor z_i for each $j \in \{1,2,3,4,5\}$

Table 4.1. System parameters in Real-time simulations

Parameter	Value
$R\ [\Omega]$	0.1
$L\ [\mathrm{H}]$	0.0025
$R_{bat}\ [\Omega]$	0.05
$L_{bat}[\mathrm{H}]$	0.001
$R_{SC}\ [\Omega]$	0.01
$L_{SC}[\mathrm{H}]$	0.001
$V_{gd}\ [\mathrm{V}]$	179.629
$V_{gq}\ [\mathrm{V}]$	0
$V_{ob}\ [\mathrm{V}]$	240
$V_{os}\ [\mathrm{V}]$	240
$R_b\ [\Omega]$	0.01
$R_s\ [\Omega]$	0.01
$i_{pv}\ [amp]$	50
$\omega\ [rad/\sec]$	377
$V_{dcref}\ [\mathrm{V}]$	500
$C_{dc}\ [F]$	0.0063

To reduce stress on the battery and lengthen its lifespan, the SC is assigned the role of handling sudden surges and changes, while the battery's role is to provide good energy flow over long time periods.

Table 4.2. Control parameters in Real-time simulations

Parameter	Value
C_1	6440
C_2	0.15
k	1981.33
K_{bat}	0.005
K_d	0.005
K_q	0.0034
K_{SC}	0.001
K_{u1}	1
K_{u2}	1
K_{u3}	1
K_{u4}	1
λ_a	0.1
m	14
p	5146.37

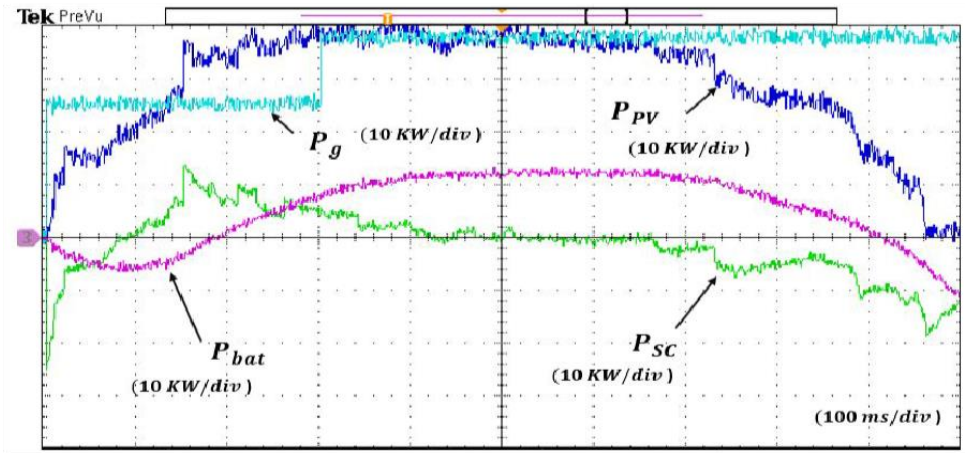

Figure. 4.2. Real-time power profiles of PV, grid, battery, and SC.

Using the method from the Appendix and the parameters from Tables I and II, we use 14 chain predictors. Then, the derivation in the Appendix implies that the system is globally asymptotically stabilized to the origin on $\mathbb{R}^5$ by the controls whose positive constants $K_{u1}, K_{u2}, K_{u3}, K_{u4}, K_d, K_q, K_{\text{bat}}$, and K_{SC} can be chosen arbitrarily. By our choices (5) of the state variables for (6), this ensures tracking of the reference states that we specify below. The control inputs have a constant delay h, and they use the five scalar valued components z_{14_j} of the 14th (and therefore last) chain predictor for $j =$

1,2,3,4,5. For the dynamics of the predictors, see the Appendix. The number of chain predictors mainly depends on the chosen delay; see the Appendix.

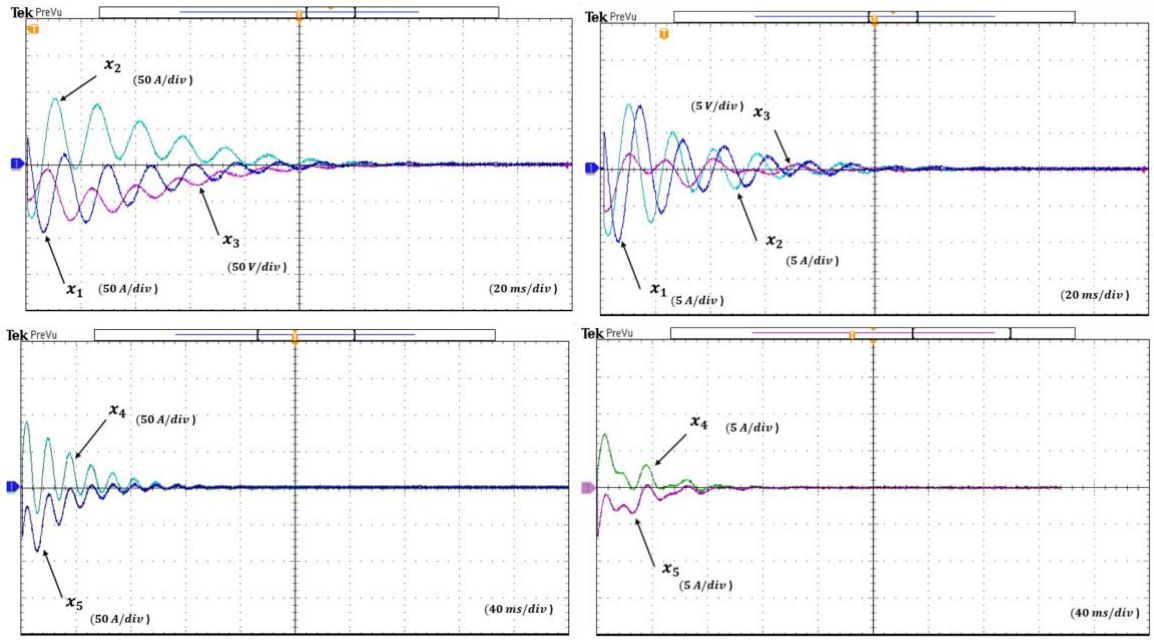

Figure. 4.3. Real-time experimental results. Top: states 1–3 using the FSA method (left) and our method (right). Bottom: states 4 and 5 using the FSA method (left) and our method (right).

$$u_1(t-h) = -K_{u1}\arctan\left(K_d\left(z_{14\_1}(t-h)V_{\text{dcref}}(t) - z_{14\_3}(t-h)I_d(t)\right)\right)$$

$$u_2(t-h) = -K_{u2}\arctan\left(K_q\left(z_{14\_2}(t-h)V_{\text{dcref}}(t) - z_{14\_3}(t-h)I_q(t)\right)\right)$$

$$u_3(t-h) = -K_{u3}\arctan\left(K_{\text{bat}}\left(z_{14\_4}(t-h)V_{\text{dcref}}(t) - z_{14\_3}(t-h)I_{\text{bat}}(t)\right)\right)$$

$$u_4(t-h) = -K_{u4}\arctan\left(K_{\text{SC}}\left(z_{14\_5}(t-h)V_{\text{dcref}}(t) - z_{14\_3}(t-h)I_{\text{SC}}(t)\right)\right) \quad (10)$$

In PEC control, it is common to choose a computational time delay close to a sampling period [70]. The sampling frequency in real-time simulations is 20kHz, which gives a sampling period (and a time delay) of $50\mu s$. When deriving our control formulas, we chose $h = 0.0001$ s. However, to show that our method works with even larger delays, we chose the delay 0.001 s in our simulations, which use the controls (10) for values of the constants in Table II, which includes

parameters not appearing in (10) but which are needed to apply the control design from the Appendix.

While small, the delay 0.001 s is significant; see, e.g., [70] for a simpler power electronics example where chain predictors stabilize a set point with the delay 0.001 s but where the same delay was shown to give large oscillations when no delay compensation is used. We also conducted real-time simulations in Section IV to show that without delay compensation, the PV/battery/SC system performance is deteriorated, and undesirable oscillations will be present. This motivates our use of chain predictors for this system.

4.4. Real-Time Simulations and Discussions

We carried out real-time simulations to evaluate the performance of the delay compensation technique for our system with the delay 0.001 s. The PV source, three-phase inverter, HESS, dc/dc converters, and the grid are modeled on an OP4510 real-time simulator from Opal-RT Technologies, Inc., operating with a Kintex7 field-programmable gate array (FPGA). The sampling frequency is 20kHz. The system and control parameters are listed in Tables I and II.

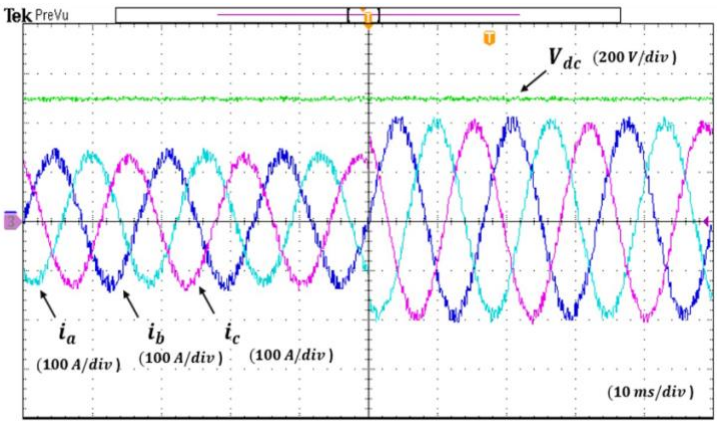

Figure. 4.4. Real-time dc-link voltage and three-phase grid currents.

The values in Table II were chosen to satisfy the requirements from (A.6) - (A.9). The PV power is obtained by using real solar data from the U.S. National Renewable Energy Laboratory (NREL) and is shown in Figure. 4.2 along with the grid, battery, and SC powers. It is noteworthy that unlike the SC power, the battery power does not contain high surges and transients. At the beginning, the reference grid power is set to 25 kW, and at $t = 0.3$ s, it is stepped up by 12.5 kW. This step change is introduced to verify the dynamic performance of our feedback controller in addition to its steady-state performance. The reference grid reactive power is set to zero. Figure. 4.3 plots the state responses using our chain predictor method versus the responses from a FSA method, which implemented the control from [71, Equation (3)] on a linearization of our bilinear x dynamics with $D = 0.001$ s and each entry of the 4×5 matrix K in [30, Equation (3)] being -0.025. We took all other parameters to be the same when we used both methods, and we used the delay 0.001 s.

Our plots show that under the FSA controller, the state variables have large oscillations before converging to zero. Oscillations in battery and SC currents adversely affect HESS lifetime. Oscillations in the dc-link voltage reduce the dc-link capacitor lifetime and mandate using semiconductor switching devices with higher voltage ratings, which are more expensive. Also, oscillations in the grid current inject voltage imbalances across the transformer and transmission line into the bulk power system, which, in turn, introduce new issues related to power quality. We show the dc-link voltage in Figure. 4.4 with the grid three phase currents. The dc-link voltage is kept at the reference value of 500 V, confirming that the power balance is maintained. The same step change can be seen in the grid three phase currents, showing an increase in the power delivered to the grid.

We extracted the execution cycle time of the two methods using monitoring blocks in real-time simulations and found that our method's implementation time is almost one quarter of that of the FSA method. This can be attributed to the computational simplicity of our method, which does not rely on distributed terms in the control.

To show the effect of delay compensation on the system performance, we carried out real-time simulations for the same system without delay compensation. Figure. 4.5 has a comparison of the state trajectories with and without delay compensation under the delay 0.001 s, where the subscript UC labels results when no delay compensation was used, which were generated using the controls (10) except with z_{14_j} replaced by x_i for $= 1,2,\dots,5$. In each plot, the system with sequential predictors achieved convergence, while the system without sequential predictors has a large divergence. It is noteworthy that these results are obtained by designing the chain predictors by choosing $h = 0.0001$ s. This illustrates that the desired convergence is achieved even when the digital implementation delay is larger than the h value in the controller equations.

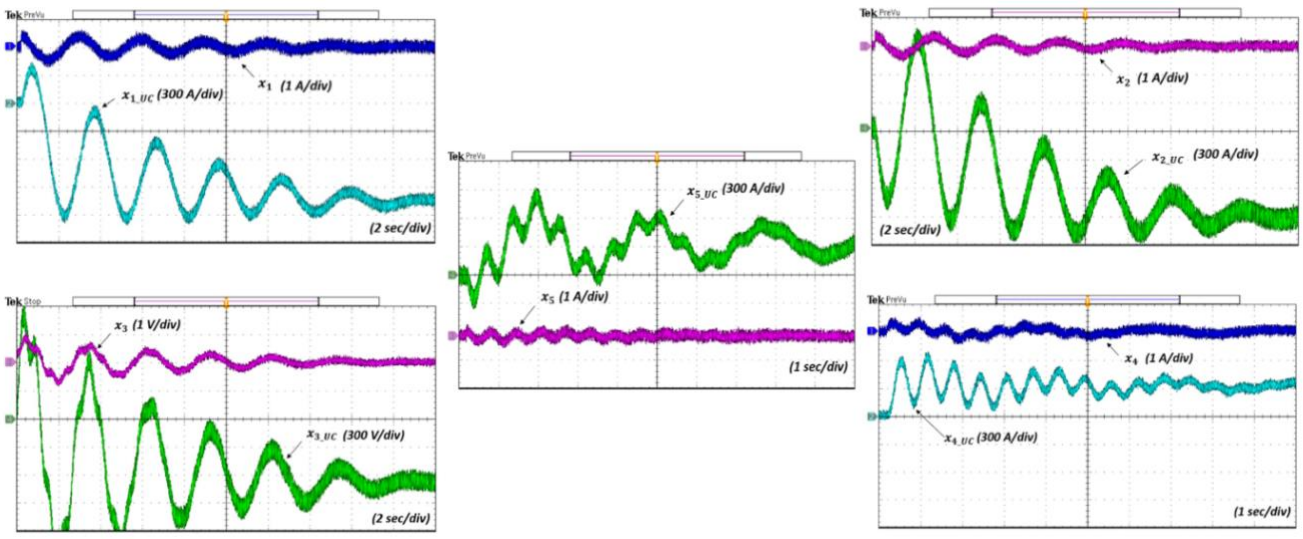

Figure. 4.5. Real-time state trajectories with and without delay compensation

4.5. Conclusion

We provided a novel delay compensating feedback control technique for a grid-connected PV/HESS based on delay-compensating chain predictors. It enjoys simplicity and global asymptotic stability in the sense of Lyapunov. Real-time simulations at steady-state and during transients verify the efficacy of our method in controlling the dynamics of the grid-connected PV/HESS and ensuring delivery of the desired power to the grid under digital implementation delays.

Chapter 5. Conclusions and Future Work

In this research, the stability issue of grid-connected hybrid PV/Battey/SC system is investigated, and a novel feedback controller is proposed to deal with time delays that due to the digital implementation of the controller. The proposed controller is based on Lyapunov theory and uses chain predictors to compensate for the digital implementation time delays. It is shown that the GAS of the system equilibrium and ISS are achieved under the proposed controller. Real-time studies are conducted to show the real-time implementation feasibility and dynamic response of the proposed feedback controller. The real-time results demonstrate the efficacy of the proposed controller in providing accurate power reference tracking and ensuring delivery of the desired power to the grid under solar source output energy and grid load variations. Comparative studies against a controller designed based on a finite spectrum assignment (FSA) approach reveal the effectiveness of our proposed method in reducing the computational complexity and the amplitude of the state variables' oscillations in real-time.

Two limitations of our method are as follows: 1) the need for values of the coefficients in the bilinear system model to design the delay compensating chain predictor control and 2) the fact that our chain predictors require knowing a value of the delay. Therefore, new theories can be developed to handle the coefficient matrices or delay uncertainties. Also, future research could study the effects of time-varying delays using generalized sequential predictor methods for time-varying delays. Last but not least, the real-time implementation feasibility of these methods could be verified through HIL or experimental studies.

Appendix A. Supporting Materials for Chapter 3

Using the definition of f_0 gives

$$\dot{\varepsilon}_1(t) = -p\varepsilon_1\left(t-\frac{h}{m}\right) + f_0\left(t+\frac{\hbar}{m}, z_1(t), u\left(t-\frac{h(m-1)}{m}\right)\right) - f\left(t+\frac{\hbar}{m}, \mathrm{x}\left(t+\frac{\hbar}{m}\right), u\left(t-\frac{h(m-1)}{m}\right), \delta\left(t+\frac{h}{m}\right)\right) \tag{A.1}$$

and

$$\dot{\varepsilon}_i(t) = -p\varepsilon_i\left(t-\frac{h}{m}\right) + p\varepsilon_{i-1}(t) + f_0\left(t+i\frac{\hbar}{m}, z_i(t), u\left(t-\frac{h(m-\mathrm{i})}{m}\right)\right) - f_0\left(t+i\frac{\hbar}{m}, z_{i-1}\left(t+\frac{\hbar}{m}\right), u\left(t-\frac{h(m-\mathrm{i})}{m}\right)\right) \tag{A.2}$$

when $i > 1$. We first study the ε_1-subsystem (A.1). The Fundamental Theorem of Calculus yields

$$\dot{\varepsilon}_1(t) = -p\varepsilon_1(t) + p\int_{t-\frac{\mathrm{h}}{m}}^{t} \dot{\varepsilon}_1(\ell)\mathrm{d}\ell + f_0\left(t+\frac{\hbar}{m}, z_1(t), u\left(t-\frac{h(m-1)}{m}\right)\right) - f\left(t+\frac{h}{m}, x\left(t+\frac{h}{m}\right), u\left(t-\frac{h(m-1)}{m}\right), \delta\left(t+\frac{h}{m}\right)\right). \tag{A.3}$$

$$\begin{aligned}\dot{v}(t) &\le -p|\varepsilon_1(t)|^2 + p\int_{t-\frac{h}{\mathrm{m}}}^{t} \varepsilon_1(t)^{\mathsf{T}}\dot{\varepsilon}_1(\ell)\mathrm{d}\ell + |\varepsilon_1(t)|k\left(\left|z_1(t)-x\left(t+\frac{h}{m}\right)\right| + \left|\delta\left(t+\frac{h}{m}\right)\right|\right)\\ &+k|\varepsilon_1(t)|\left|\delta\left(t+\frac{h}{m}\right)\right| \le (k-p)|\varepsilon_1(t)|^2 + k|\varepsilon_1(t)|\left|\delta\left(t+\frac{h}{m}\right)\right|\\ &+p\int_{t-\frac{h}{m}}^{t}\left[\frac{c_1}{2}|\varepsilon_1(t)|^2 + \frac{1}{2c_1}|\dot{\varepsilon}_1(\ell)|^2\right]\mathrm{d}\ell\\ &= \left(k-p+\frac{phc_1}{2m}\right)|\varepsilon_1(t)|^2 + \frac{p}{2c_1}\int_{t-\frac{h}{m}}^{t}|\dot{\varepsilon}_1(\ell)|^2\,\mathrm{d}\ell + k|\varepsilon_1(t)|\left|\delta\left(t+\frac{h}{m}\right)\right|.\end{aligned} \tag{A.4}$$

Next, note that (A.1) gives the following for all $\ell \ge 0$:

$$|\dot{\varepsilon}_1(\ell)| \le p\left|\varepsilon_1\left(\ell-\frac{h}{m}\right)\right| + f_0\left|\begin{matrix}\left(\ell+\frac{h}{m}, z_1(\ell), u\left(\ell-\frac{h(m-1)}{m}\right)\right)\\ -f\left(\ell+\frac{h}{m}, x\left(\ell+\frac{h}{m}\right), u\left(\ell-\frac{h(m-1)}{m}\right), \delta\left(\ell+\frac{h}{m}\right)\right)\end{matrix}\right|$$
$$\le p\left|\varepsilon_1\left(\ell-\frac{b}{m}\right)\right| + k\left(|\varepsilon_1(\ell)| + \left|\delta\left(\ell+\frac{h}{m}\right)\right|\right),$$

by Assumption 2. Hence, Young's Inequality gives

$$\begin{aligned}|\dot{\varepsilon}_1(\ell)|^2 \le\ & (1+C_2)\mathrm{p}^2\left|\varepsilon_1\left(\ell-\frac{h}{m}\right)\right|^2 \\ & +\left(1+\frac{1}{c_2}\right)k^2(|\varepsilon_1(\ell)|^2 + |\delta(\ell+h/m)|^2 \\ & +2|\varepsilon_1(\ell)|\left|\delta\left(\ell+\frac{h}{m}\right)\right|\Big) \\ \le\ & (1+C_2)p^2|\varepsilon_1(\ell-h/m)|^2 \\ & +\left(1+\frac{1}{C_2}\right)k^2\left(\left(1+\frac{\lambda_a}{4}\right)|\varepsilon_1(\ell)|^2\right. \\ & \left.+(1+4/\lambda_a)]\delta(\ell+h/m)|^2\right)\end{aligned}$$

for all $t \ge 0$. Therefore, (A. 4) gives

$$\begin{aligned}&\dot{v}(t) \le \left(k-p+\frac{phc_1}{2\pi i}\right)|\varepsilon_1(t)|^2 + k|\varepsilon_1(t)\ \|\delta\left(t+\frac{h}{m}\right)| \\ &+\frac{p^3(1+C_2)}{2C_1}\int_{t-\frac{2\,\mathrm{h}}{\mathrm{m}}}^{t-\frac{\mathrm{h}}{\mathrm{m}}}|\varepsilon_1(\ell)|^2\,\mathrm{d}\ell \\ &+\frac{pk^2}{2C_1}\left(1+\frac{1}{C_2}\right)\left(1+\frac{\lambda_{\mathrm{a}}}{4}\right)\int_{t-\frac{\mathrm{h}}{\mathrm{m}}}^{t}|\varepsilon_1(\ell)|^2\,\mathrm{d}\ell \\ &+\frac{pk^2}{2C_1}\left(1+\frac{1}{c_2}\right)\left(1+\frac{4}{\lambda_{\mathrm{a}}}\right)\int_{t}^{1+\frac{h}{m}}|\delta(\ell)|^2\,\mathrm{d}\ell\end{aligned} \tag{A.5}$$

for all $t \ge \frac{h}{m}$. Since Young's inequality also gives

$$k|\varepsilon_1(t)||\delta(t+h/m)| \le \frac{\lambda_a}{2}|\varepsilon_1(t)|^2 + \frac{k^2}{2\lambda_a}|\delta(t+h/m)|^2, \tag{A.6}$$

we can use (A.6) to upper bound the last term in (A.5) and our choice of p and finally our choice of v to get

$$\dot{v}(t) \le -k|\varepsilon_1(t)|^2 + \frac{p^3(1+C_2]}{2C_1}\int_{t-2h/m}^{t-h/m} |\varepsilon_1(\ell)|^2 \, \mathrm{d}\ell$$
$$+\frac{pk^2}{2C_1}\left(1+\frac{1}{C_2}\right)\left(1+\frac{\lambda_{\mathrm{a}}}{4}\right)\int_{l-h/\mathrm{m}}^{t} |\varepsilon_1(\ell)|^2 \, \mathrm{d}\ell + \bar{M}|\delta|^2_{[t,t+h/m]} \tag{A.7}$$

where $\bar{M}$ is defined in (6).

Recalling our choice of $\mu(\varepsilon_{1,\mathrm{t}})$from (16), it follows that for all $t \ge h/m$, we have

$$\frac{d}{\mathrm{dt}}\mu(\varepsilon_{1,t}) \le -2kv(\varepsilon_1(t)) + \bar{M}|\delta|^2_{[\mathrm{t},t+h/\mathrm{m}]} - \bar{C}(1+\lambda_{\mathrm{a}})\int_{\mathrm{t}-2h/\mathrm{m}}^{\mathrm{t}} v(\varepsilon_1(\ell))\mathrm{d}\ell$$
$$+\bar{C}\left(\int_{t-2\mathrm{h/m}}^{t} v(\varepsilon_1(\ell))\mathrm{d}\ell + \frac{2h(1+2\lambda_{\mathrm{a}})}{\mathrm{m}} v(\varepsilon_1(\mathrm{t}))\right) \tag{A.8}$$

This gives

$$\frac{d}{dt}\mu(\mathcal{E}_{1,t}) \le 2k\left[-1+\frac{\mathrm{h}\bar{C}}{k\mathrm{m}}(1+\lambda_a)\right]v(\mathcal{E}_1(t)) - \lambda_a\bar{C}\int_{t-2\ \mathrm{h/m}}^{t} v(\mathcal{E}_1(\ell))\mathrm{d}\ell + \bar{M}|\delta|^2_{[t,t+\mathrm{h/m}]}.$$

(A.9)

Therefore, our condition (8) from our theorem and our choice of ϵ_0 in (6), combined with the bound $\tilde{\mu}(\varepsilon_{1,t}) \le v(\mathcal{E}_1(t)) + 2\left(1+\frac{h\bar{C}(1+\lambda_a)}{m}\right)\int_{\mathrm{t}-2\ \mathrm{h/m}}^{t} v(\mathcal{E}_1(\ell))\mathrm{d}\ell$, give controls along all trajectories of the ε_1 dynamics. Similarly, since there is no δ in the z system, (A.2) and the relation $2rs \le \lambda_a r^2/4 + 4s^2/\lambda_0$ for all $r \ge 0$ and $s \ge 0$ give

$$\begin{aligned}
|\dot{\varepsilon}_\iota(\ell)|^2 \le\ & (1+C_2)p^2|\mathcal{E}_i(\ell-h/m)|^2 \\
& +\left(1+\frac{1}{C_2}\right)(k|\varepsilon_i(\ell)| + p|\varepsilon_{i-1}(\ell)|)^2 \\
\le\ & (1+C_2)p^2|\mathcal{E}_i(\ell-h/m)|^2 \\
& +\left(1+\frac{1}{C_2}\right)k^2(1+\lambda_a/4)|\varepsilon_i(\ell)|^2 \\
& +\left(1+\frac{1}{C_2}\right)p^2(1+4/\lambda_a)|\varepsilon_{i-1}(\ell)|^2
\end{aligned} \tag{A.10}$$

for any $i \in \{2,3,\dots,m\}$.

This implies that the function $\mu(\mathcal{E}_{i,t})$ from (18) satisfies the following for all $t \geq h/m$:

$$\begin{aligned}
\frac{d}{dt}\mu(\mathcal{E}_{i,t}) \leq \quad & -\epsilon_0\tilde{\mu}(\mathcal{E}_{i,t}) + p|\mathcal{E}_i(t)||\mathcal{E}_{i-1}(t)| \\
& + C_2^{\#}\int_{t-h/m}^{t} |\mathcal{E}_{i-1}(\ell)|^2 \, \mathrm{d}\ell \\
\leq \quad & -\epsilon_0\tilde{\mu}(\mathcal{E}_{i,t}) + \tfrac{\epsilon_0}{4}|\mathcal{E}_i(t)|^2 + \tfrac{p^2}{\epsilon_0}|\mathcal{E}_{i-1}(t)|^2 \\
& + C_2^{\#}\int_{t-h/m}^{t} |\mathcal{E}_{i-1}(\ell)|^2 \, \mathrm{d}\ell \\
\leq \quad & -\tfrac{\epsilon_0}{2}\tilde{\mu}(\mathcal{E}_{i,t}) + \tfrac{p^2}{\epsilon_0}|\mathcal{E}_{i-1}(t)|^2 \\
& + C_2^{\#}\int_{t-h/m}^{t} |\mathcal{E}_{i-1}(\ell)|^2 \, \mathrm{d}\ell
\end{aligned} \tag{A.11}$$

where the second inequality used Young's inequality and

$C_2^{\sharp} = \left(1 + \frac{1}{C_2}\right)\frac{p^3}{2C_1}(1 + 4/\lambda_a)$, which proves the lemma.

Appendix B. Supporting Materials for Chapter 4

We explain how to apply the chain predictor approach to derive our controls. Part of the derivation involves specializing results of previous works for bilinear systems with arbitrarily long constant delays to cases where the uncertainties are not present and so where the conclusion is uniform global asymptotic stability instead of the input-to-state stability (ISS). However, as in our original work, we express our assumptions in terms of ISS. Therefore, we write system as follows:

$$\dot{x}(t) = A(t)x(t) + \sum_{i=1}^{4} u_i(t-h)(B_i x(t) + G_i(t)) \tag{A.1}$$

with the matrices $B_i = [B_{ijk}]$ having the entries $B_{113} = 1/L, B_{131} = -1/C_{\mathrm{dc}}, B_{223} = 1/L, B_{232} = -1/C_{\mathrm{dc}}, B_{334} = -1/C_{\mathrm{dc}}, B_{343} = 1/L_{\mathrm{bat}}, B_{435} = -1/C_{\mathrm{dc}}$, and $B_{453} = 1/L_{\mathrm{SC}}$, and all other entries of the B_i 's being zero, where B_{ijk} is the entry in the j th row and k th column of B_i for $i = 1,2,3,4$, $j = 1,2,3,4,5, k = 1,2,3,4,5$, and

$$A(t) = \begin{bmatrix} -\frac{R}{L} & \omega & \frac{D_{d(t)}}{L} & 0 & 0 \\ -\omega & -\frac{R}{L} & \frac{D_{q(t)}}{L} & 0 & 0 \\ -\frac{D_{d(t)}}{c_{dc}} & -\frac{D_{q(t)}}{c_{dc}} & 0 & -\frac{D_{bat(t)}}{c_{dc}} & -\frac{D_{sc(t)}}{c_{dc}} \\ 0 & 0 & \frac{\mathrm{D_{bat(t)}}}{\mathrm{L_{bat}}} & -\frac{R_b^{\#}}{L_{bat}} & 0 \\ 0 & 0 & \frac{D_{sc}(t)}{L_{SC}} & 0 & -\frac{R_s^{\#}}{L_{SC}} \end{bmatrix} \tag{A.2}$$

where $R_{\mathrm{b}}^{\#} = R_{\mathrm{bat}} + R_b$ and $R_s^{\#} = R_{\mathrm{SC}} + R_S$, and with

$$G_1(t) = \begin{bmatrix} \frac{V_{\mathrm{dcref}}(t)}{L} \\ 0 \\ -\frac{I_d(t)}{C_{\mathrm{dc}}} \\ 0 \\ 0 \end{bmatrix},\ G_2(t) = \begin{bmatrix} 0 \\ \frac{V_{\mathrm{dcref}}(t)}{L} \\ -\frac{I_q(t)}{C_{\mathrm{dc}}} \\ 0 \\ 0 \end{bmatrix}$$

$$G_3(t) = \begin{bmatrix} 0 \\ 0 \\ -\frac{I_{\mathrm{bat}}(t)}{C_{\mathrm{dc}}} \\ \frac{V_{\mathrm{dcref}}(t)}{L_{\mathrm{bat}}} \\ 0 \end{bmatrix},\ G_4(t) = \begin{bmatrix} 0 \\ 0 \\ -\frac{I_{\mathrm{SC}}(t)}{C_{\mathrm{dc}}} \\ 0 \\ \frac{V_{\mathrm{dcref}}(t)}{L_{\mathrm{SC}}} \end{bmatrix}. \tag{A.3}$$

The main requirement for the zero uncertainties case specialized to the bilinear dynamic (A.1) is the as follows, where $\mathcal{B}_{\bar{\epsilon}} \subseteq \mathbb{R}^5$denotes the closed ball of radius $\bar{\epsilon} > 0$ centered at the origin, $|\cdot|$ denotes the usual Euclidean norm and the corresponding matrix operator two norm, u_{si} denotes the i th component of u_s for $i = 1,2,3,4$, and $0_{m\times n}$ denotes the $m \times n$ matrix whose entries are all zeros for all m and n.

Assumption 1: There are a compact neighborhood $\mathcal{U} \subseteq \mathbb{R}^4$ of $0_{4\times 1}$, a continuous function $u_s: [0,\infty) \times \mathbb{R}^5 \to \mathcal{U}$ that is globally Lipschitz in its second variable uniformly in its first variable, and a constant $\bar{\epsilon} > 0$, such that the system

$$\dot{x}(t) = A(t)x(t) + \sum_{i=1}^{4} u_{si}\big(t, x(t) + \epsilon(t)\big)\big(B_i x(t) + G_i(t)\big) \tag{A.4}$$

with disturbance ϵ satisfies the ISS property for all piecewise continuous functions ϵ that are valued in disturbance set $\mathcal{B}_{\bar{\epsilon}}$. Also, $u_s(t, 0_{5\times 1}) = 0_{4\times 1}$ for all $t \geq 0$.

The preceding assumption means that u_s ensures the required ISS conditions when there is no delay, and, therefore, can act as a preliminary or nominal control that we will transform into our delay compensating controller using the sequential predictors that we present below. Later, here, we show how to construct u_s and $\mathcal{U}$ that satisfy the requirements of Assumption 1. We now set

$$k = |A|_\infty + \bar{U} \sum_{i=1}^{4} |B_i| \tag{A.5}$$

for any bound $\bar{U}$ on the elements of the set $\mathcal{U}$ from Assumption 1, where $|\cdot|_\infty$ is the sup-norm. The statement of the theorem in [70] also requires that the time-varying coefficient matrices (which in our case are A and the G_i 's) are continuous, but the proof of the previous main result shows that this continuity requirement can be replaced by the requirements that all entries of these coefficient matrices are bounded and piecewise continuous. This will allow us to apply the method in our case, where the jump in P_g and the relation $(3/2)V_{gd}I_d = P_g$ produce a discontinuous trajectory component I_d; see Figure. 4.2.

Fixing a positive integer m and any constants $h > 0, C_1 \in (0, 2m/h), C_2 > 0$, and $\lambda_a > 0$, and any constant $\bar{\epsilon}$ satisfying Assumptions 1, and

$$p = \frac{m(4k+\lambda_a)}{2m - hC_1} \tag{A.6}$$

$$\bar{C} = \frac{p}{C_1} max\left\{p^2(1+C_2), k^2\left(1+\frac{1}{C_2}\right)\left(1+\frac{\lambda_a}{4}\right)\right\} \tag{A.7}$$

which will be positive constants under condition (A.8), we use the following special case of the main result, which provides the required chain predictors for our control design, where we use the class $\mathcal{KL}$ of functions. $|.|_J$ is the supremum over intervals J in the usual Euclidean norm.

Lemma 1: Let Assumption 1 hold, and assume that

$$m > \frac{h\bar{C}(1+\lambda_a)}{k} \tag{A.8}$$

Then, for the control u_s from Assumption 1, system (A.1), in closed loop with the feedback control

$$u(t) = u_s(t + h, z_m(t)) \tag{A.9}$$

where z_m is the last n components of the state of the system

$$\begin{aligned} \dot{z}_i(t) = \quad & A\left(t + \frac{ih}{m}\right) z_i(t) \\ & + \sum_{i=1}^{4} \Phi_i(t, z_m, i)\left[B_i z_i(t) + G_i\left(t + \frac{ih}{m}\right)\right] \\ & - p\left[z_i\left(t - \frac{h}{m}\right) - z_{i-1}(t)\right],\ 1 \le i \le m \end{aligned} \tag{A.10}$$

and $z_0 = x$ and

$$\Phi(t, z_m, i) = u_s(t + h - h(m - i)/m, z_m(t - h(m - i)/m)) \tag{A.11}$$

admits a function $\beta_d \in \mathcal{KL}$, such that all solutions $(x, z) : [t_0 - 2h, \infty) \to \mathbb{R}^{5(m+1)}$ of the preceding closed loop system for all $t_0 \ge h/m$ satisfy

$$|x(t)| \le \beta_d\left(|x|_{[t_0-2h, t_0+h/m]} + |z|_{[t_0-2h, t_0+h/m]}, t - t_0\right) \tag{A.12}$$

for all $t \ge t_0$, where $z = (z_1, \ldots, z_m)$.

The choices of the above parameters, such as C_1, C_2, and λ_a, are used to determine β_d [70], and so impact the convergence rate. The dynamics (A.10) are m chain predictors, which, in our simulations, are $m = 14$ dynamic extension with the state z_i of the i th extension having dimension $n = 5$ for $i = 1, \ldots, 14$. To find u_s from Assumption 1 needed to apply Lemma 1, we use Lemma 2 , which follows from combining [70, Remark 4] with the choices $\sigma_i(s) = c_{1i}\arctan(c_{2i}s)$ for $i = 1, \ldots, 4$ for positive constants c_{ji} for $j = 1,2$, and which uses standard definitions of properness and positive definiteness.

Lemma 2: Let A and the matrix valued functions B_i and G_i for $i = 1,2,3,4$ be as above. Assume that there are constants $c_i \geq 0$ and a symmetric positive definite matrix $P \in \mathbb{R}^{5\times5}$, such that the following hold with $V(x) = x^\top Px$.

1) Along all solutions of $\dot{x} = A(t)x$, we have

$$\dot{V} \leq -\sum_{i=1}^{5} c_i x_i^2(t) \qquad \text{at all times } t \geq 0. \tag{A.13}$$

2) The functions $V(x)$ and

$$\sum_{i=1}^{5} c_i x_l^2 + \sum_{i=1}^{4} |x^\top PB_i x + x^\top PG_i(t)| \tag{A.14}$$

are uniformly proper and positive definite.

3) The functions

$$\mathcal{H}_i(t,x) = \frac{x^\top\left(PB_i + B_i^\top P\right) + G_i^\top(t)P}{1+4\left(x^\top PB_i x + x^\top PG_i(t)\right)^2} \tag{A.15}$$

are bounded for $i = 1, \dots, 4$. Choose a positive value

$$\mathcal{H}_* \geq 2\,\mathrm{s}\ \{|\mathcal{H}_i(t,x)|: x \in \mathbb{R}^5, t \geq 0, 1 \leq i \leq 4\}. \tag{A.16}$$

Then, for any constants $\bar{\omega}_i > 0$ and $v_i > 0$ for $i = 1,2, \dots, 4$ and $\bar{\epsilon} \in \left(0, \pi/(2\mathcal{H}_*)\right)$, and with the choice

$$u_s(t,x) = -\left(\bar{\omega}_1 \arctan\left(v_1 M_1(t,x)\right), \dots, \bar{\omega}_4 \arctan\left(v_4 M_4(t,x)\right)\right) \tag{A.17}$$

where

$$M_i(t,x) = x^\top PB_i x + x^\top PG_i(t), \quad \text{for } 1 \leq i \leq 4$$

the system (A.1) satisfies Assumption 1 with the product set

$$\mathcal{U} = [-\pi\bar{\omega}_1/2, \pi\bar{\omega}_2/2] \times \cdots \times [-\pi\bar{\omega}_c/2, \pi\bar{\omega}_c/2].$$

We next show why the requirements of Lemma 2 are satisfied for our dynamics (A.1), which will allow us to conclude that Lemmas 1 and 2 provide the controls (10). We choose the diagonal matrix $P = (1/2)\mathrm{diag}\{L, L, C_{\mathrm{dc}}, L_{\mathrm{bat}}, L_{\mathrm{SC}}\}$ for the Lyapunov function $V(x) = x^{\top}Px$ and the constants $c_1 = c_2 = R, c_3 = 0, c_4 = R_{\mathrm{bat}}$, and $c_5 = R_{\mathrm{SC}}$ in Lemma 2. Using the facts that $\inf_{t\geq 0}|I_{\mathrm{bat}}(t)| > 0$ and that the entries of G_i 's are bounded and piecewise continuous, we can check that the assumptions of Lemma 2 are satisfied when we choose the values from Tables 4.1 and 4.2. Hence, by choosing the function u_s from Lemma 2 in Lemma 1, we obtain controls.

Appendix C. Copyright Information

Copyright information for Chapter 3

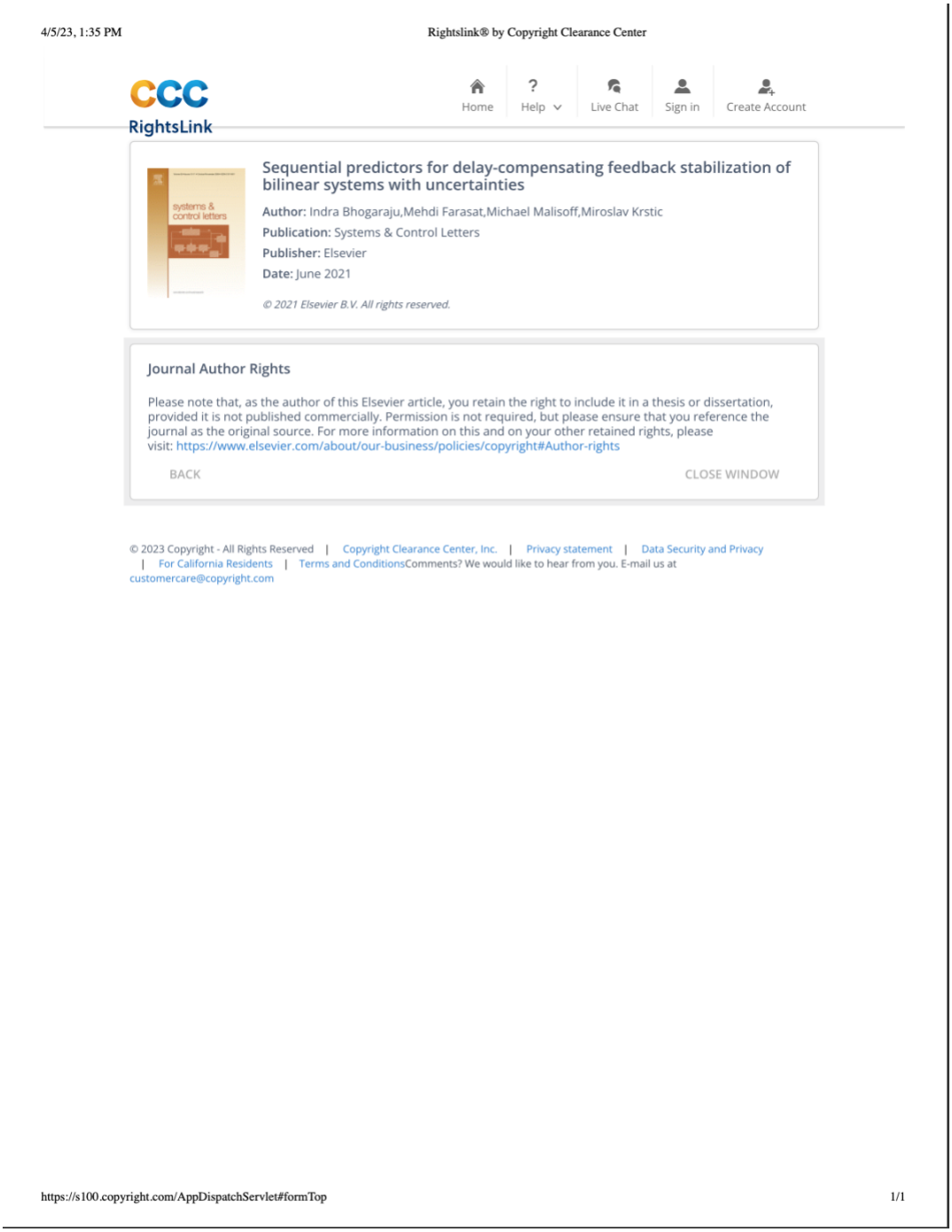

4/5/23, 1:35 PM Rightslink® by Copyright Clearance Center

CCC RightsLink

Home | Help | Live Chat | Sign in | Create Account

Sequential predictors for delay-compensating feedback stabilization of bilinear systems with uncertainties

Author: Indra Bhogaraju,Mehdi Farasat,Michael Malisoff,Miroslav Krstic

Publication: Systems & Control Letters

Publisher: Elsevier

Date: June 2021

© 2021 Elsevier B.V. All rights reserved.

Journal Author Rights

Please note that, as the author of this Elsevier article, you retain the right to include it in a thesis or dissertation, provided it is not published commercially. Permission is not required, but please ensure that you reference the journal as the original source. For more information on this and on your other retained rights, please visit: https://www.elsevier.com/about/our-business/policies/copyright#Author-rights

BACK CLOSE WINDOW

© 2023 Copyright - All Rights Reserved | Copyright Clearance Center, Inc. | Privacy statement | Data Security and Privacy | For California Residents | Terms and ConditionsComments? We would like to hear from you. E-mail us at customercare@copyright.com

https://s100.copyright.com/AppDispatchServlet#formTop 1/1

Copyright information for Chapter 4

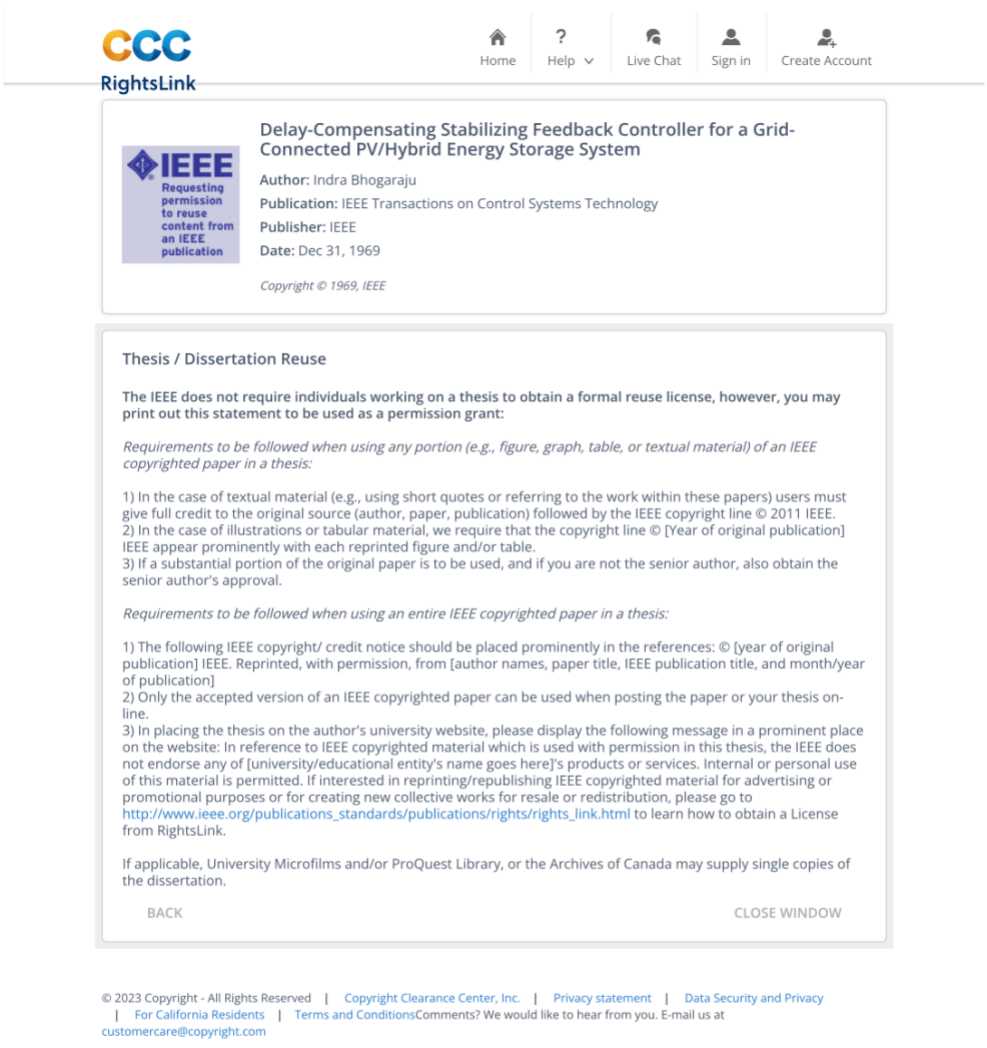

RightsLink

Home | Help | Live Chat | Sign in | Create Account

IEEE Requesting permission to reuse content from an IEEE publication

Delay-Compensating Stabilizing Feedback Controller for a Grid-Connected PV/Hybrid Energy Storage System

Author: Indra Bhogaraju

Publication: IEEE Transactions on Control Systems Technology

Publisher: IEEE

Date: Dec 31, 1969

Copyright © 1969, IEEE

Thesis / Dissertation Reuse

The IEEE does not require individuals working on a thesis to obtain a formal reuse license, however, you may print out this statement to be used as a permission grant:

Requirements to be followed when using any portion (e.g., figure, graph, table, or textual material) of an IEEE copyrighted paper in a thesis:

1) In the case of textual material (e.g., using short quotes or referring to the work within these papers) users must give full credit to the original source (author, paper, publication) followed by the IEEE copyright line © 2011 IEEE.
2) In the case of illustrations or tabular material, we require that the copyright line © [Year of original publication] IEEE appear prominently with each reprinted figure and/or table.
3) If a substantial portion of the original paper is to be used, and if you are not the senior author, also obtain the senior author's approval.

Requirements to be followed when using an entire IEEE copyrighted paper in a thesis:

1) The following IEEE copyright/ credit notice should be placed prominently in the references: © [year of original publication] IEEE. Reprinted, with permission, from [author names, paper title, IEEE publication title, and month/year of publication]
2) Only the accepted version of an IEEE copyrighted paper can be used when posting the paper or your thesis on-line.
3) In placing the thesis on the author's university website, please display the following message in a prominent place on the website: In reference to IEEE copyrighted material which is used with permission in this thesis, the IEEE does not endorse any of [university/educational entity's name goes here]'s products or services. Internal or personal use of this material is permitted. If interested in reprinting/republishing IEEE copyrighted material for advertising or promotional purposes or for creating new collective works for resale or redistribution, please go to http://www.ieee.org/publications_standards/publications/rights/rights_link.html to learn how to obtain a License from RightsLink.

If applicable, University Microfilms and/or ProQuest Library, or the Archives of Canada may supply single copies of the dissertation.

BACK CLOSE WINDOW

References

[1] N. Kumar, T. K. Saha and J. Dey, "Sliding-Mode Control of PWM Dual Inverter-Based Grid-Connected PV System: Modeling and Performance Analysis," in *IEEE Journal of Emerging and Selected Topics in Power Electronics*, vol. 4, no. 2, pp. 435-444, June 2016.

[2] B. Wang, U. Manandhar, X. Zhang, H. B. Gooi and A. Ukil, "Deadbeat Control for Hybrid Energy Storage Systems in DC Microgrids," in *IEEE Transactions on Sustainable Energy*, vol. 10, no. 4, pp. 1867-1877, Oct. 2019.

[3] Z. Afshar, M. M. Zadeh and S. M. T. Bathaee, "Sliding Mode Control of Grid-connected Inverters Using Inverter Output Current," *2019 IEEE International Conference on Environment and Electrical Engineering and 2019 IEEE Industrial and Commercial Power Systems Europe (EEEIC / I&CPS Europe)*, Genova, Italy, 2019.

[4] C. Qi, X. Chen, P. Tu and P. Wang, "Cell-by-Cell-Based Finite-Control-Set Model Predictive Control for a Single-Phase Cascaded H-Bridge Rectifier," in IEEE Transactions on Power Electronics, vol. 33, no. 2, pp. 1654-1665, Feb. 2018.

[5] Y. Zhu and J. Fei, "Disturbance Observer Based Fuzzy Sliding Mode Control of PV Grid Connected Inverter," in IEEE Access, vol. 6, pp. 21202-21211, 2018.

[6] S. Rojas and A. Gensior, "Prediction of the Average Value of State Variables for Modulated Power Converters Considering the Modulation and Measuring Method," in *IEEE Transactions on Industrial Electronics*, vol. 63, no. 8, pp. 5209-5220, Aug. 2016.

[7] D. Zhu, S. Zhou, X. Zou, Y. Kang and K. Zou, "Small-Signal Disturbance Compensation Control for LCL-Type Grid-Connected Converter in Weak Grid," in *IEEE Transactions on Industry Applications*, vol. 56, no. 3, pp. 2852-2861, May-June 2020.

[8] H. Li, W. Wu, M. Huang, H. Shu-hung Chung, M. Liserre and F. Blaabjerg, "Design of PWM-SMC Controller Using Linearized Model for Grid-Connected Inverter With LCL Filter," in *IEEE Transactions on Power Electronics*, vol. 35, no. 12, pp. 12773-12786, Dec. 2020.

[9] N. Altin, S. Ozdemir, H. Komurcugil and I. Sefa, "Sliding-Mode Control in Natural Frame With Reduced Number of Sensors for Three-Phase Grid-Tied LCL-Interfaced Inverters," in *IEEE Transactions on Industrial Electronics*, vol. 66, no. 4, pp. 2903-2913, April 2019.

[10] L. Guo, N. Jin, Y. Li and K. Luo, "A Model Predictive Control Method for Grid-Connected Power Converters Without AC Voltage Sensors," in *IEEE Transactions on Industrial Electronics*, vol. 68, no. 2, pp. 1299-1310, Feb. 2021.

[11] E. T. Andrew, K. H. Ahmed and D. Holliday, "A New Model Predictive Current Controller for Grid-Connected Converters in Unbalanced Grids," *in IEEE Transactions on Power Electronics*, vol. 37, no. 8, pp. 9175-9186, Aug. 2022.

[12] R. Errouissi, H. Shareef and F. Awwad, "Disturbance Observer-Based Control for Three-Phase Grid-Tied Inverter With LCL Filter," in *IEEE Transactions on Industry Applications*, vol. 57, no. 5, pp. 5411-5424, Sept.-Oct. 2021.

[13] N. N. Nam, N. -D. Nguyen, C. Yoon and Y. I. Lee, "Disturbance Observer-Based Robust Model Predictive Control for a Voltage Sensorless Grid-Connected Inverter With an LCL Filter," in *IEEE Access*, vol. 9, pp. 109793-109805, 2021.

[14] D. Palomares, C. Hernandez, J. vaquero, N. Vazquez and H. Lopez, "Lyapunov-Based Control Strategy for a Multi-Function Single-Phase Inverter for Photovoltaic Systems," *2018 14th International Conference on Power Electronics (CIEP)*, Cholula, Puebla, Mexico, 2018.

[15] C. Meza, D. Biel, D. Jeltsema and J. M. A. Scherpen, "Lyapunov-Based Control Scheme for Single-Phase Grid-Connected PV Central Inverters," in IEEE Transactions on Control Systems Technology, vol. 20, no. 2, pp. 520-529, March 2012.

[16] H. Komurcugil and O. Kukrer, "Lyapunov-based control for three-phase PWM AC/DC voltage-source converters," in *IEEE Transactions on Power Electronics*, vol. 13, no. 5, pp. 801-813, Sept. 1998.

[17] K. Biju and R. Ramchand, "A Modified Lyapunov Function Based Control Strategy for Single Phase Cascaded H-bridge Multilevel Inverter with Nonlinear Loads," *2019 IEEE Industry Applications Society Annual Meeting*, Baltimore, MD, USA, 2019.

[18] S. Bayhan, H. Komurcugil, H. Abu-Rub and Y. Liu, "A Lyapunov Stability Theorem Based Control Strategy for Single-Phase Neutral-Paint-Clamped Quasi - Impedance Source Inverter with LCL Filter," *IECON 2018 - 44th Annual Conference of the IEEE Industrial Electronics Society*, Washington, DC, USA, 2018.

[19] S. R. Sanders and G. C. Verghese, "Lyapunov-based control for switched power converters," in *IEEE Transactions on Power Electronics*, vol. 7, no. 1, pp. 17-24, Jan. 1992.

[20] H. Komurcugil and O. Kukrer, "A new control strategy for single-phase shunt active power filters using a Lyapunov function," in *IEEE Transactions on Industrial Electronics*, vol. 53, no. 1, pp. 305-312, Feb. 2006.

[21] S. Rahmani, A. Hamadi and K. Al-Haddad, "A Lyapunov-Function-Based Control for a Three-Phase Shunt Hybrid Active Filter," in *IEEE Transactions on Industrial Electronics*, vol. 59, no. 3, pp. 1418-1429, March 2012.

[22] I. Sefa, S. Ozdemir, H. Komurcugil and N. Altin, "An Enhanced Lyapunov-Function Based Control Scheme for Three-Phase Grid-Tied VSI With LCL Filter," in *IEEE Transactions on Sustainable Energy*, vol. 10, no. 2, pp. 504-513, April 2019.

[23] S. S. Seyedalipour and G. B. Gharehpetian, "A Lyapunov-function-based control strategy for stable operation of a grid-connected DC microgrid with variable generations and energy storage," *2016 21st Conference on Electrical Power Distribution Networks Conference (EPDC)*, Karaj, Iran, 2016.

[24] S. Seyedalipour, S. Bayhan and H. Komurcugil, "A Lyapunov-Function-Based Control Strategy for Distributed Generations in Hybrid AC/DC Microgrids," *2019 IEEE 28th International Symposium on Industrial Electronics (ISIE)*, Vancouver, BC, Canada, 2019.

[25] A. S. Md. Khalid Hasan, I. Bhogaraju, M. Farasat and M. Malisoff, "Lyapunov Function-Based Stabilizing Control Scheme for Wireless Power Transfer Systems with LCC Compensation Network," *2021 IEEE Applied Power Electronics Conference and Exposition (APEC)*, 2021.

[26] *F. Saccomanno, Electric Power Systems: Analysis and Control. New York, NY, USA: Wiley, 2003.*

[27] G. Besançon, D. Georges, Z. Benayache, Asymptotic state prediction for continuous-time systems with delayed input and application to control, in: Proceedings of the European Control Conference, Kos, Greece, 2007, pp. 1786–1791.

[28] F. Cacace, A. Germani, Output feedback control of linear systems with input, state and output delays by chains of predictors, Automatica 85 (2017) 455–461.

[29] F. Mazenc, M. Malisoff, Stabilization of nonlinear time-varying systems through a new prediction-based approach, IEEE Trans. Automat. Control 62 (6) (2017) 2908–2915.

[30] J. Weston, M. Malisoff, Sequential predictors under time-varying feedback and measurement delays and sampling, IEEE Trans. Automat. Control 64 (7) (2019) 2991–2996.

[31] D. Elliot, Bilinear Control Systems, Springer Science and Business Media, New York, NY, 2009.

[32] S. Ghosh, J. Ruths, Structural control of single-input rank one bilinear systems, Automatica 64 (2016) 8–17.

[33] R. Mohler, Bilinear Control Processes with Applications to Engineering, Ecology, and Medicine, Academic Press, New York, NY, 1973.

[34] T. Ahmed-Ali, E. Fridman, F. Giri, M. Kahelras, F. Lamnabhi-Lagarrigue, L. Burlion, Observer design for a class of parabolic systems with large delays and sampled measurements, IEEE Trans. Automat. Control 65 (5) (2020) 2200–2206.

[35] F. Cacace, A. Germani, C. Manes, Exponential stabilization of linear systems with time-varying delayed state feedback via partial spectrum assignment, Systems Control Lett. 69 (2014) 47–52.

[36] F. Cacace, A. Germani, C. Manes, Predictor-based control of linear systems with large and variable measurement delays, Internat. J. Control 87 (4) (2014) 704–714.

[37] F. Cacace, F. Conte, A. Germani, G. Palombo, Delay identification for a class of nonlinear systems, Internat. J. Control 89 (1) (2016) 2350–2359.

[38] F. Cacace, F. Conte, A. Germani, G. Palombo, Optimal control of linear systems with large and variable input delays, Systems Control Lett. 89 (2016) 1–7.

[39] F. Cacace, F. Conte, A. Germani, P. Pepe, Stabilization of strict-feedback nonlinear systems with input delay using closed-loop predictors, Internat. J. Robust Nonlinear Control 26 (16) (2016) 3524–3540.

[40] F. Cacace, F. Conte, A. Germani, Output transformations and separation results for feedback linearizable delay systems, Internat. J. Control 91 (4) (2018) 797–812.

[41] A. Selivanov, E. Fridman, Predictor-based networked control under uncertain transmission delays, Automatica 70 (2016) 101–108.

[42] A. Selivanov, E. Fridman, Delayed point control of a reaction-diffusion PDE under discrete-time point measurements, Automatica 96 (2018) 224–233.

[43] Y. Zhu, E. Fridman, Predictor methods for decentralized control of large-scale systems with input delays, Automatica 116 (2020) 108903.

[44] M. Malisoff, F. Zhang, Robustness of adaptive control under time delays for three-dimensional curve tracking, SIAM J. Control Optim. 35 (4) (2015) 2203–2236.

[45] N. Bekiaris-Liberis, M. Krstic, Predictor-feedback stabilization of multiinput nonlinear systems, IEEE Trans. Automat. Control 62 (2) (2017) 516–531.

[46] M. Krstic, Delay Compensation for Nonlinear, Adaptive, and PDE Systems, Birkhauser, Boston, MA, 2009.

[47] M. Krstic, Input delay compensation for forward complete and feedforward nonlinear systems, IEEE Trans. Automat. Control 55 (2) (2010) 287–303.

[48] H. Khalil, Nonlinear Systems, third ed., Prentice Hall, Upper Saddle River, NJ, 2002.

[49] M. Di Ferdinando, P. Pepe, E. Fridman, Exponential input-to-state stability of globally Lipschitz time-delay systems under sampled-data noisy output feedback and actuation disturbances, Internat. J. Control (2020) in press.

[50] F. Mazenc, M. Malisoff, S.-I. Niculescu, Reduction model approach for linear time-varying systems with delays, IEEE Trans. Automat. Control 59 (8) (2014) 2068–2082.

[51] G. Mirzaeva, G. Goodwin, and C. Townsend, "Dealing with linear and nonlinear time delays under model predictive control of power electronic inverters," in *Proc. IEEE Int. Conf. Automatica (ICA-ACCA)*, Oct. 2016, pp. 1–8.

[52] Y. He, X. Wang, X. Ruan, D. Pan, and K. Qin, "Hybrid active damping combining capacitor current feedback and point of common coupling voltage feedforward for LCL-type grid-connected inverter," *IEEE Trans. Power Electron.*, vol. 36, no. 2, pp. 2373–2383, Feb. 2021.

[53] X. Zhang, P. Chen, C. Yu, F. Li, H. T. Do, and R. Cao, "Study of a current control strategy based on multisampling for high-power grid connected inverters with an LCL filter," *IEEE Trans. Power Electron.*, vol. 32, no. 7, pp. 5023–5034, Jul. 2017.

[54] D. Pan, X. Ruan, C. Bao, W. Li, and X. Wang, "Capacitor-currentfeedback active damping with reduced computation delay for improving robustness of LCL-type grid-connected inverter," *IEEE Trans. Power Electron.*, vol. 29, no. 7, pp. 3414–3427, Jul. 2014.

[55] C. Zou, B. Liu, S. Duan, and R. Li, "Influence of delay on system stability and delay optimization of grid-connected inverters with LCL filter," *IEEE Trans. Ind. Informat.*, vol. 10, no. 3, pp. 1775–1784, Aug. 2014.

[56] W. Xia and J. Kang, "Stability of LCL-filtered grid-connected inverters with capacitor current feedback active damping considering controller time delays," *J. Modern Power Syst. Clean Energy*, vol. 5, no. 4, pp. 584–598, Jul. 2017.

[57] T. Jin, X. Shen, T. Su, and R. C. C. Flesch, "Model predictive voltage control based on finite control set with computation time delay compensation for PV systems," *IEEE Trans. Energy Convers.*, vol. 34, no. 1, pp. 330–338, Mar. 2019.

[58] B. Cao, L. Chang, and R. Shao, "Predictive current controller for singlephase grid-connected VSIs with compensation for time-delay effect and system uncertainty," *IEEE J. Emerg. Sel. Topics Power Electron.*, vol. 6, no. 4, pp. 1761–1768, Dec. 2018.

[59] A. Calle-Prado, S. Alepuz, J. Bordonau, P. Cortes, and J. Rodriguez, "Predictive control of a back-to-back NPC converter-based wind power system," *IEEE Trans. Ind. Electron.*, vol. 63, no. 7, pp. 4615–4627, Jul. 2016.

[60] Y. Zhang, J. Liu, H. Yang, and S. Fan, "New insights into model predictive control for three-phase power converters," *IEEE Trans. Ind. Appl.*, vol. 55, no. 2, pp. 1973–1982, Apr. 2019.

[61] P. Cortes, J. Rodriguez, C. Silva, and A. Flores, "Delay compensation in model predictive current control of a three-phase inverter," *IEEE Trans. Ind. Electron.*, vol. 59, no. 2, pp. 1323–1325, Feb. 2012.

[62] M. Ajmeri and A. Ali, "Modified Smith predictor and controller for unstable first order processes," in *Proc. Indian Control Conf. (ICC)*, Jan. 2017, pp. 397–402.

[63] Y. Wang, W. Xie, X. Wang, and D. Gerling, "A precise voltage distortion compensation strategy for voltage source inverters," *IEEE Trans. Ind. Electron.*, vol. 65, no. 1, pp. 59–66, Jan. 2018.

[64] T. Liu, C. Xia, X. Gu, and T. Shi, "An observer-based finite control set model predictive control for three-phase power converters," *Math. Problems Eng.*, vol. 2014, pp. 1–9, Mar. 2014.

[65] S.-K. Kim and C. K. Ahn, "Learning algorithm-based offset-free onestep time-delay compensation for power converter and motor drive system applications," *IEEE Trans. Ind. Informat.*, vol. 16, no. 6, pp. 3789–3796, Jun. 2020.

[66] S.-K. Kim, "Offset-free one-step ahead state predictor for power electronic applications using robust proportional–integral observer," *IEEE Trans. Ind. Electron.*, vol. 63, no. 3, pp. 1763–1770, Mar. 2016.

[67] F. Mazenc, M. Malisoff, and Z. Lin, "Further results on input-to-state stability for nonlinear systems with delayed feedbacks," *Automatica*, vol. 44, no. 9, pp. 2415–2421, Sep. 2008.

[68] Z. Artstein, "Linear systems with delayed controls: A reduction," *IEEE Trans. Autom. Control*, vol. AC-27, no. 4, pp. 869–879, Aug. 1982.

[69] R. Katz and E. Fridman, "Sub-predictors and classical predictors for finite-dimensional observer-based control of parabolic PDEs," *IEEE Control Syst. Lett.*, vol. 6, pp. 626–631, 2022.

[70] I. Bhogaraju, M. Farasat, M. Malisoff, and M. Krstic, "Sequential predictors for delay-compensating feedback stabilization of bilinear systems with uncertainties," *Syst. Control Lett.*, vol. 152, Jun. 2021, Art. no. 104933.

[71] M. Krstic, "Compensation of infinite-dimensional actuator and sensor dynamics," *IEEE Control Syst. Mag.*, vol. 30, no. 1, pp. 22–41, Feb. 2010.

[72] E. D. Sontag, "Input to state stability: Basic concepts and results," in Nonlinear and Optimal Control Theory, P. Nistri and G. Stefani, Eds.

Vita

Indra Narayana Sandilya Bhogaraju received his undergraduate degree from GITAM University, Visakhapatnam, India, in 2015 and his M.Sc. degree in Electrical Engineering (Power) from the University of Houston, TX, USA, in 2017. He is pursuing his Ph.D. degree in Electrical Engineering (Power) with the Department of Electrical and Computer Engineering, Louisiana State University, LA, USA, with anticipated graduation in May 2023. He has more than five years of experience in research, presented talks on multiple occasions, and published several papers as a part of his research journey. His research areas include grid integration of renewables, electric vehicles, modeling and control of power electronics converters, and nonlinear control theory. After completion of his doctoral degree, he plans to become a research scientist in the field of power electronics.